ELECTROCHEMISTRY OF 3D PRINTED ARCHITECTURES

Wasiq Jahangir

Submitted in fulfilment of the requirements of the Manchester Metropolitan University for the degree of Master of Science (by Research)

August 2018

School of Science and the Environment

Division of Chemistry and Environmental Science

Manchester Metropolitan University

Table of Contents

LIST OF FIGURES

LIST OF ABBREVIATIONS

AM	Additive manufacturing
K^0	Heterogenous rate transfer constant
3D	Three dimensional
CAD	Computer-aided design
FDM	Fused deposition modelling
SLS	Stereolithographic sintering
DIR	Direct ink writing
PLA	Polylactic acid
CPC	Conductive polymeric composites
LP	Linear polymer
PS	Polystyrene

PE	Polyethylene
PVC	Polyvinyl chloride
BP	Branched polymer
CP	Crosslinked polymer
NP	Network polymer
TP	Thermoplastic Polymer
PRC	Particle reinforced composite
FRC	Fibre reinforced composites
MMC	Metal matrix composites
CMC	Ceramics matrix composite
PMC	Polymeric matrix composite
CB	Carbon black
C	Carbon
H	Hydrogen
C□H	Bond between carbon and hydrogen
ABS	Acrylonitrile butadiene styrene
ABS-PC	Acrylonitrile butadiene styrene-Polycarbonate blend
MVI	Melt viscosity index
NG	Nano-graphite Mesoporous (500 nm)
3DE	Three-dimensionally printed electrodes
TF	Thin films
FTIR	Fourier transform infrared spectroscopy
SP	Super P carbon black

ABSTRACT

Recently, the fused deposition modelling (FDM) based additive manufacturing technique has gained the attraction for producing three-dimensionally printed electrochemical architecture (ECA). The FDM printer is fed by a thermoplastic filament which passes through a heated extruder to melt and cast it in the desired shape. In this research work, we explored the effect of 3D printing on the electrochemical behaviour of the conductive polymeric composites (CPC). The composites filament containing different electroactive materials were subjected to the electrochemical characterisation. The Polylactic acid (PLA) blend with the graphene, nano-graphite (NG), and carbon black (SP) showed that the bulk filament (BF) has higher heterogonous electron rate transfer constant (K^0) (towards hexaamine-ruthenium(iii) chloride) as compared to their respective 3D printed electrode. Moreover, when the different parts of the same filament subjected to the voltammetry studies, all parts showed different K^0 values. For example, tail-1, middle, tail-2, and the 3DE of the 20% SP/PLA showed the K^0 of 2.824×10^{-4}, 8.28×10^{-4}, 4.88×10^{-4} and 2.39×10^{-4} cm s^{-1} respectively. These variable values of K^0 proved that the homogeneity of the BF will be a challenge in future. The K^0 of the BF of the 20% graphene/PLA and 20% SP/PLA composites were 3.2×10^{-4} and 2.824×10^{-4} cm s^{-1} respectively. These values are comparable to that of the conventional electrodes proving that in future these 3D printers can be employed in the manufacturing of the ECA. The composites with higher percentage filler loading showed the higher K^0 value because of the higher conductivity. Moreover, the thin films with single polymer blend such as ABS filled with the electroactive material showed better electrochemical performance as compared with the CPC of ABS-PC. This trend validates that the individual polymer blend with the electroactive material is better for producing electrochemical architectures as compared to the blend with two immiscible polymers.

1. Introduction

1.1 Additive Manufacturing

Recently, the three-dimensional printers (3D-printers) have emerged as a concept of the small industrial units capable of replacing the old technologies associated with fabrication operations.(1) The additive manufacturing (AM) also known as 3D-printing is a process of converting the computer-aided design (CAD) into a product. The CAD is transformed to the layered model using a specially designed software, the printer program then decodes this complex geometry to produce the structure using a layer by layer deposition approach.(2) The stacking of these layers gives a unique advantage of building the complex 3D-structure without a scrape. In 1988, Charles Hull patented his invention known as stereolithography apparatus (SLA) which led the foundation of the 3D printer industry.(3, 4) Later, scientists had developed many different technological processes which can 3D print varieties of materials. The AM has the following many unique benefits over the traditional production processes.

- The AM is a cost-effective single step process to directly convert the material into the desired geometry without producing a scrap.(5) There is no cost associated with the production and handling of expensive moulds.(6)
- The portability is a distinct benefit, and these machines can easily be transported to the desired environment.(7)
- The 3D printing can be employed in the automation of manufacturing industries capable of reducing the skills required for the process handling.(6)

These unique features have convinced industrial and government-backed defence authorities to increase their investment in the AM.(8) In the expert opinion, the total market size of the 3D printing industry will reach 20 billion dollars by 2020.(9) In a decade of research, the

advanced 3D printers have proven beneficial in the aeronautical, biomedical, energy, electroanalytical, and other engineering sectors.(10) Presently, the numerous 3d printing techniques are available in the market such as SLA, Direct ink writing (DIW), fused deposition method (FDM), selective and laser sintering (SLS).(11) These techniques have broadened the scope of 3D printing by enabling the range of materials to be fabricated, i.e., free-form fabrication is not limited to the polymeric materials anymore.(11) In general, all these AM techniques have a few main components which are associated with several engineering sectors from software to materials science.(12) The process starts with the computer program to generate the CAD as an initial source of command which is processed into a layered architect by printer's operating software followed by decoding into the machine language instructions.(13) These electronic codes are then delivered to a circuitry unit for operating the cartesian robot and material feeding system for building a required structure.(13) The printer's program is designed to controls the feeding system for a specific material, i.e., only those materials can be processed which have similar properties.(14)

1.2 Fused Deposition Modelling:

The FDM printer is fed by a thermoplastic filament which passes through a heated extruder for subsequent melting. The fused plastic will then pass a nozzle and reach to a print area as shown in **Figure 1.1**. The motion of a feeding system is controlled by the computer controlled cartesian robot enabling them to build 3D motifs.(15) Recently, the 3D printing has drawn much attention as a manufacturing process for the ECA which has tested in batteries, super-capacitors, hydrogen generation reaction, oxygen evolution reaction and electro-analysis.(10) The SLS based 3D printers can be employed to produce the complex structure of the metals and ceramics with control of the micro-porosity.(16) However, the beneficial features of the

polymer-based 3D printers concerning the speed, efficiency, and precision are persuading researchers to explore its ability to develop electro-responsive assemblies.(17) The electrical conductivity of the structure is a pre-requisite to be utilised in an electrochemical application. In general, the polymers are insulators and can be compounded with the conductive filler to make it an electrical conductor.(18) The characteristics of the conductive polymeric composite (CPC) not only depends upon its constituents but also rely on a compounding process adopted to make a blend.(19) In this regard, it is desirable to study the polymeric materials, composites, and the compounding operations for the successful implementation of 3D printed CPC as ECA.

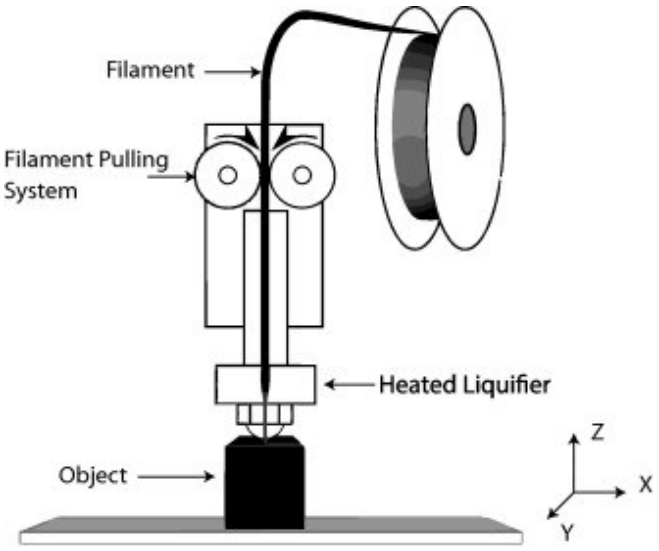

Figure 1.1 Illustration of the Working of FDM 3D printers. Reproduced from reference (20)

1.3 Polymeric material:

All solid materials are classified into three major categories, i.e., metals, polymers, and ceramics.(21, 22) The polymeric materials are composed of covalently bonded organic molecules (also known as monomers) arranged in long chains. The weak van der wall forces exist between these chains.(23) These London dispersion forces are highly influenced by the length, structure, and functional groups of the polymeric molecule.(23) The properties that a polymer exhibit is a function of its molecular structure.(23) On the basis of the physical properties and molecular structures, the polymers are further subdivided into different types.

The thermoplastic polymers (TP) turned into liquid upon heating. Whereas thermosetting polymers are those polymers when subjected to heat, they become hard, and upon further heating, they start to degrade.(24) In general, the FDM requires melting for printing a polymeric structure and can only process TP.(25) The polymeric molecular structure has a considerable influence on its mechanical and thermal properties. The feeding system of FDM is calibrated on the physical properties of the polymers which in fact is a function of their molecular structures.(26)

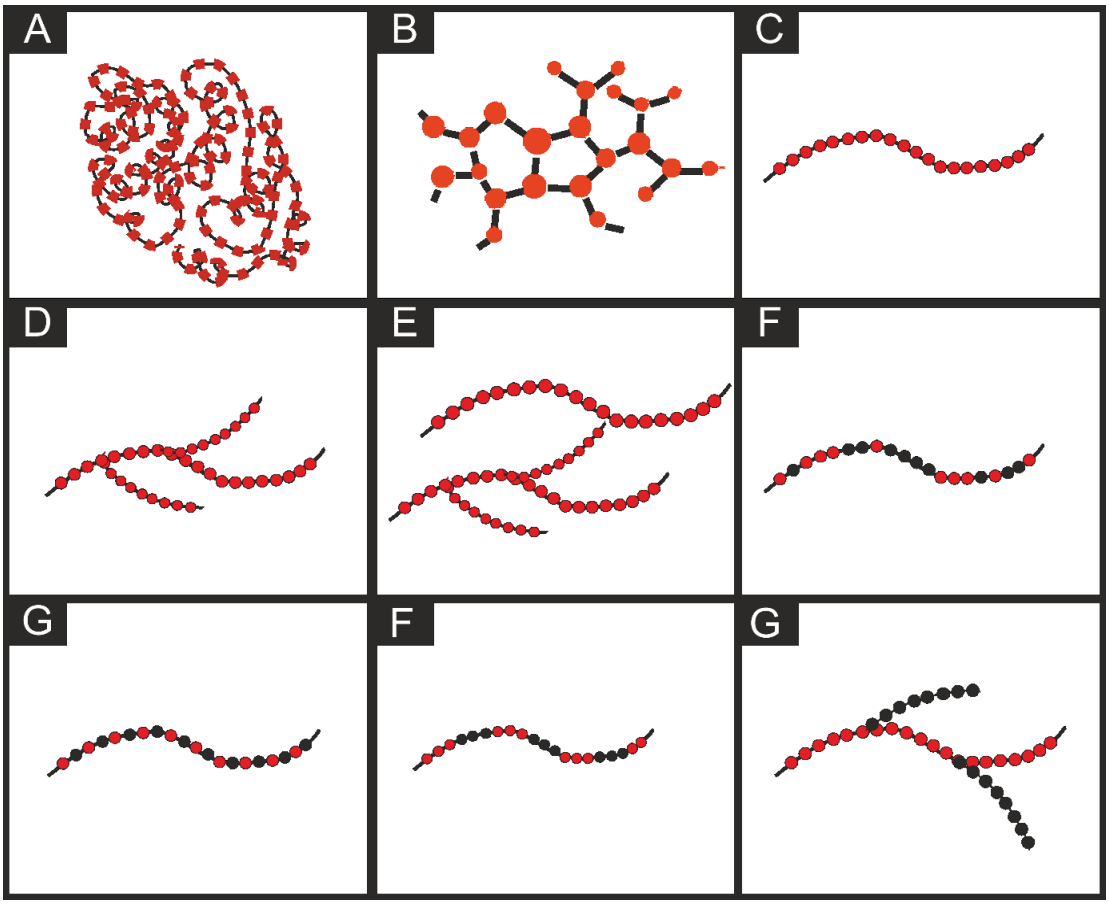

Figure 1.2 (A) Polymeric chain structure, (B) network polymer, (C) linear polymer, (D) branched polymer, (E) crosslinked polymer, (F) random copolymer, (G) alternating copolymer, (H) block copolymer, and (I) graft polymer (Black and red beads are representing two different monomers).

1.3.1 Types of the polymeric molecular structures:

1.3.1.1 Linear polymer:

Those polymers in which the monomers join linearly to form a single chain are known as a linear polymer (LP). The polystyrene (PS), polyethene (PE), polyvinyl chloride (PVC) are the examples of LP.(27)

1.3.1.2 Branched polymers:

In branched polymers (BP) the molecular chains are attached to form a branch structure as shown in **Figure 1.2 (D)**. The linear structure can be branched by creating side reactions during production. Consequently, the density and melting point of the BP becomes higher, and the compressibility of these polymer reduces.(27, 28)

1.3.1.3 Crosslinked polymers:

In crosslinked Polymer (CP) the molecular chains are attached by a covalent bond as illustrated in **Figure 1.2 (E).** In CP, the degree of covalent bonds between the chains is higher compared to the BP. The crosslinking will enhance the mechanical and thermal properties of a polymer. However, elasticity will decrease as compared to a linear polymer.(29)

1.3.1.4 Network polymer:

In Network polymers (NP), the monomers are attached to form a three-dimensional network structure as shown in **Figure 1.2 (B)**. In fact, polymers which have the high degree of crosslinking are termed as network polymers. The network polymers exhibit superior mechanical and thermal stability.(30)

1.3.1.5 Copolymers:

Those polymers with different monomers in one chain are known as copolymers.(31) To understand the structure of a copolymer, consider a molecule which is made up of two distinct monomers as shown in **Figure 1.2 (F)**. The reaction conditions and polymerisation process can control the sequence and fraction of monomers in a polymeric chain. (31) (**Figure 1.2** (F), (G), (H) and (I) had showed some of the possible sequences between the monomers). The structure produced by the random dispersion of the monomers is known as a random copolymer. A copolymer in which two monomers arranged themselves on alternating positions is called an alternating copolymer. Whereas, the block polymers have blocks of the monomers on alternating positions. The last type of copolymer is a graft polymer, in which

homo-polymers chains are grafted together with other chains in the form of branches.(31) (All these structures are illustrated in **Figure 1.2**) The feeding system of FDM is calibrated on the physical properties of polymers which in fact is a function of their molecular structure. All these polymers have different physical properties, and it is difficult to design a single FDM based 3D printer which can able to print all thermoplastic polymers.(25, 26) Furthermore, the molecular structure control enables to design polymeric materials with the desired properties, but these polymers are still not suitable in many applications.(32) Consequently, the scientist has explored the blends of solid materials known as a composite.(32)**Error! Reference source not found.**

1.4 Composites:

The composites are the combination of two or more materials. Usually, they consist of two phases, the continuous phase which encapsulates other is known as a matrix, while other is known as a dispersed phase.(33) The composite properties are the function of the characteristics of dispersed and a matrix material.(34) The composites are beneficial in many engineering applications where traditional materials are not suitable or economically feasible to use.(32) The composites based on the orientation, shape and the distribution of the dispersed phase can be classified into different types.(35) **Figure 1.3** is about the general classification of composites.

1.4.1 Types of composite:

1.4.1.1 Particle reinforced composite:

In particle reinforced composites (PRC), the solid particles are dispersed in a matrix.(35) Based on the physical parameters of the particle, the PRC can further be sub-divided into two types, i.e. large particle composite (LPRC) and dispersion strengthened composite (DSC). When large-sized filler particles are added in the matrix, then they are termed as LPRC. Whereas, in DSC the filler is dispersed uniformly in the matrix phase.(36, 37)

1.4.1.2 Fibre reinforced composite:

In fibre reinforced composites (FRC), the fibrous shaped fillers are added in a matrix. (35) Their characteristics not only depend upon the fibre material but also on its orientation within the matrix phase.(37, 38) Based on the orientation of fibres these composites are sub-

classified into two categories, i.e. continuous and discontinuous FRC as shown in **Figure 1.3**.(37, 38)

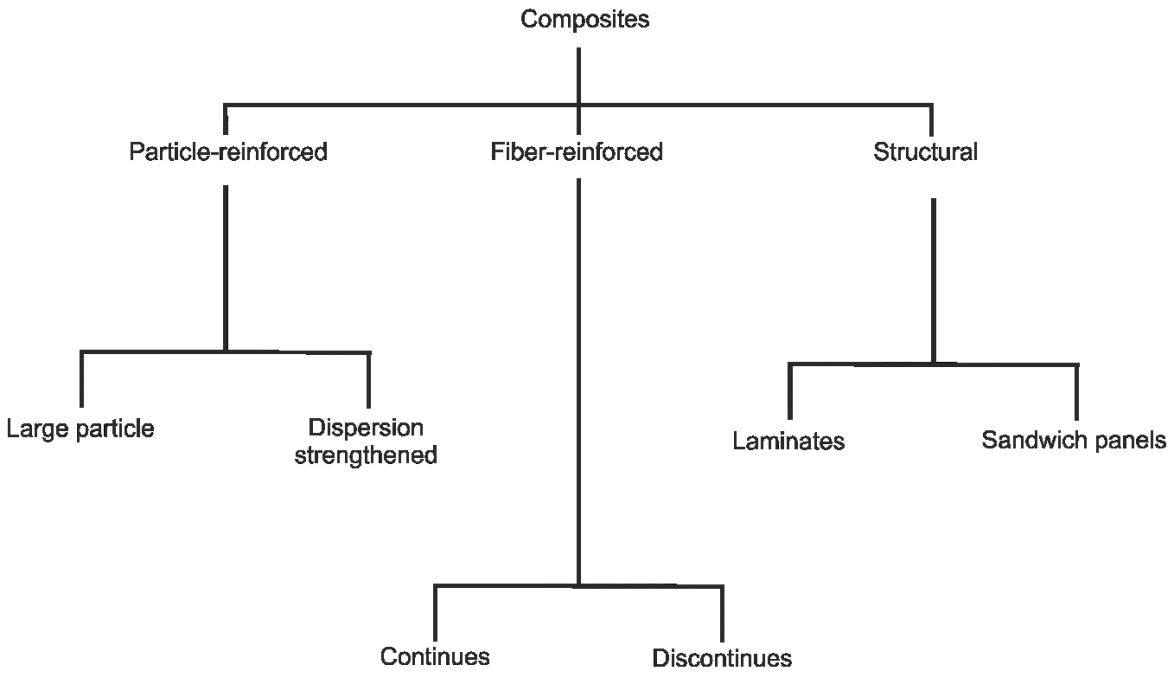

Figure 1.3 General classification of the composites

Those FRC in which fibre phase is dispersed continuously in the same orientation are termed as continuous fibre reinforced composite. In contrast, those FRC in which fibres are aligned randomly are known as discontinuous fibre reinforced composite. (38, 39)

1.4.1.3 Structural composites:

The structural composite (SC) is composed of two different homogenous composites aligned in alternating directions throughout the structure.(40) The properties of SC rely on the constituents and their geometry in which they are layered together. The SC is sub-classified into two main groups known as sandwich panel (SP) and laminar composites (LC). These composites are extensively being used in aircraft, roof floor, and wall insulation.(40, 41)

Above discussed composite classification are based on the characteristics of the dispersed phase in the matrix materials. Composites can also be categorised by the nature of a matrix

material, i.e. metal-matrix composites (MMC), ceramic matrix composites (CMC), and polymer-matrix composites (PMC).(35)

1.4.1.4 Metal matrix composites:

Those composites in which matrix phase is a metal or metallic alloy are known as MMC.(42) The filler with high melting point and fractural strength are usually melt-blended with the metallic material.(43) The MMC are useful in many applications including aerospace and transportation industries. However, they are expensive to produce as they can either processed by melting or through powder metallurgy.(43)

1.4.1.5 Ceramic matrix composites:

The CMC are based on ceramic material and can efficiently be utilised in harsh environments.(43) CMC are the best candidate for many automobile components and gas turbine engines due to extraordinary strength and resistant to the electrochemical deterioration.(43) However, the cost of these composites is high because they are produced by melting or powder metallurgy.(43, 44)

1.4.1.6 Polymer matrix composites:

Composites with the polymeric matrix are called polymeric matrix composites (PMC). They are lightweight, low cost, and are easy to produce.(43) Due to these benefits, the PMC are being utilised in many applications including aeroplane to household construction material.(45)

In FDM, the plastic filament is fed as a source of material, and only particulate filled polymeric composite can easily be fabricated into the filament form.(25, 26) Moreover, this research work was conducted to probe the effect of the 3D printing on the electrochemical response of the polymeric electrodes. In this regard, it was desirable to study the conductive polymeric blends and effect of the processing on their conductive behaviour.

2. The conductance mechanism in the polymeric composites:

The polymeric materials are insulators except for the few intrinsically conducting polymers.(45) Recently, the polymeric composite filled with the conductive particles has drawn much attention as a mouldable conductive substance.(46) The conductance through conductive polymeric composites (CPC) depends on the filler nature and its dispersion

characteristics.(46) Many theories and models have already been proposed to explain the conducting process through CPC. The classical models are primarily based on the percolation and quantum mechanical tunnelling effect.(47) Recently, few researchers elaborated that the conductance through CPC is a complex function of many physical and chemical factors which includes surface energy, size, shape, conductivity, and surface chemistry of the filler particles.(48) Whereas, the blending technique used in the manufacturing of the composite can also affect its conductive behaviour.(49)

2.1 Percolation theory:

The percolation theory applies to all inhomogeneous systems, which are composed of the non-conducting and conducting materials.(47) If we keep adding filler to the plastic, at a specific ratio, the concentration of the particles will be enough to make random contacts throughout the composite. This phenomenon is called Percolation, and the weight/volume percentage of filler at which composite starts conductance is called the percolation threshold.(50, 51) In the past, many different scientists tried to explain percolation theoretically and factually. Aharoni(52) proposed that percolation occurs when the average contact points per particle reaches to two. Janzen(53, 54) based on experimental data derived the equation for finding out a volume of the filler at percolation.

$$V = \frac{1}{1 + 0.6z\rho\varepsilon} \tag{2.1}$$

Whereas V is the volume of the filler at percolation threshold, ρ is the filler density, ε is the specific pore volume and z is the coordination number of the particle in the polymeric matrix. Whereas z is the coordination number of the particles in the polymeric matrix. Kirkpatrick(51) explained the conductivity after the percolation threshold obeys the general law and is given by

$$\sigma = \sigma_o (V - V_p)^D \tag{2.2}$$

Where σ is the conductivity of composites at filler volume V. While, σ_o is the conductivity at the percolation threshold with filler volume V_p. D is the constant whose value depends upon the physical characteristic of particles. Bueche(55) identified that the s-shaped graph exists between the conductivity and the filler percentage (as shown in **Figure 2.1**). According to Bueche, the resistivity of the composite can be expressed as

$$\frac{\rho}{\rho_m} = \frac{\rho_f}{(1-V)\rho_f + V\omega\rho_m} \quad (2.3)$$

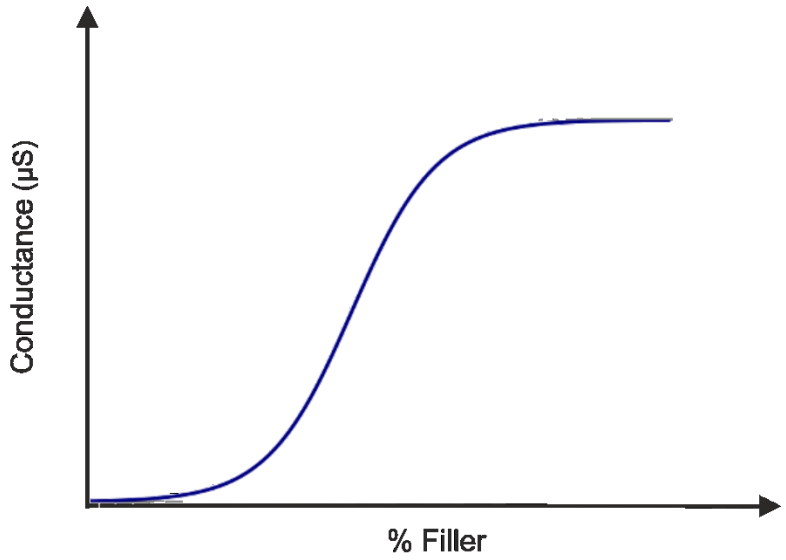

Figure 2.1 Sigmoidal relationship between the filler concentration and conductance of CPC (55)

ρ, ρ_m and ρ_f are the resistivity of the polymer, mixture, and conducting particles respectively. Whereas, V is the volume fraction of the conductive phase, and ω is the factor which depends upon the sub-factors f and α. Whereas, f is the coordination number of the particle and α is the probability of the particles to contact each other. Sumita(56) conducted the thermodynamic calculations to relate the structure of the polymer with percolation. The proposed model was based on the interfacial interaction between the particles and polymer molecules. Sumita(56) suggested that when the interfacial energies (g*) of the particles becomes much higher than that of the polymeric molecules, they start to aggregate to form a conductive path.

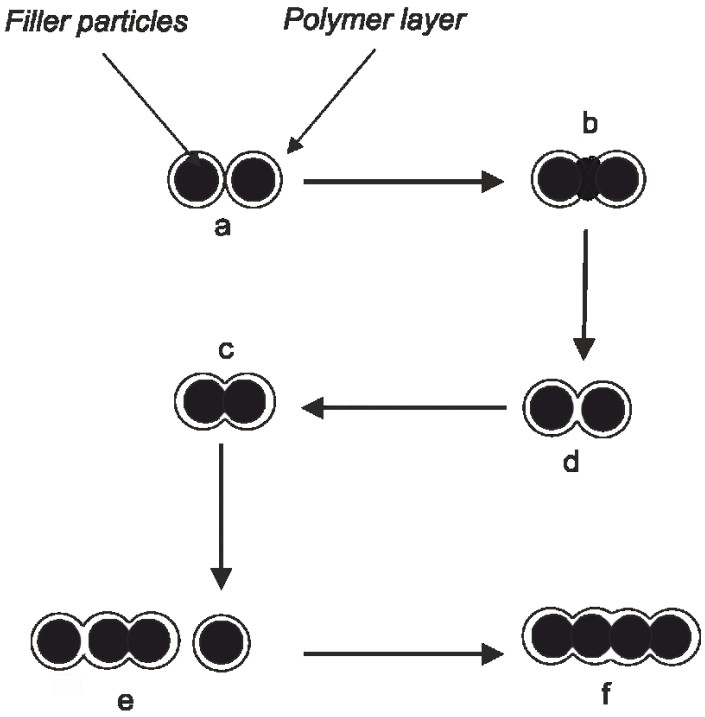

Figure 2.2 (a) Polymer thin layer surrounded the filler particle, (b) the start of the deformation of the polymer layer, (c) the particles are in contact with each other, (e) and (f) is the final stage in which polymer makes contacts with particles.

Wessling(57) proposed another model whose mechanism is shown in **Figure 2.2**. The model explains that during mixing, the conductive filler particles gets surrounded by the absorbing polymer layer (20nm). Below the percolation threshold, the filler particles are distributed evenly in the polymer phase. When the concentration reaches the percolation, the compression forces produced during mixing will destroy the adsorbed polymer layer of the particles, and they will start to percolate.

These percolation models are suggesting that the conductivity of the CPC depends upon many different factors. The optimisation of FDM 3D printer for producing CPC architectures demands much effort which is not only specific to the material science but also for the computation engineering to design complex algorithms.(25)

2.2 Quantum tunnelling effect:

The flow of electrons through CPC is governed by many different phenomena, i.e., percolation, thermal expansion (internal energy), and Quantum tunnelling effect.(47) The electrons in the atom become free to move when excited to the valence band. When the

internal energy of the particle is increased, it will generate free electrons.(58) In CPC, the insulating material encapsulates the conductive particles within the polymeric matrix. The mechanical distortion can make these particles closer such that the excited electron can jump to other particles and this creates a channel for electron flow. This phenomenon for electricity flow is known as quantum tunnelling effect.(59, 60) In percolation particles make contacts, but in quantum tunnelling effect these particles stay closer without having physical contact.(47)

3. Carbon particles-filled polymeric composites:

Carbon is one of the most abundant elements in the universe and occurs in many different crystalline and amorphous structures.(61) The graphite, diamond, fullerene, graphene and carbon nanotubes are the crystalline forms of the carbon. Whereas, the carbon black is the example of an amorphous structure.(62) The classification of the carbon material is illustrated in **Figure 3.1**.

3.1 Carbon black:

Carbon black (CB) is the amorphous forms of the carbon and are useful in many applications.(63) CB is the carbonaceous particles produced when aromatic hydrocarbons (liquids or gaseous) undergoes incomplete combustions at high temperature and pressure. When the hydrocarbons are subjected to heat under a limited supply of oxygen, the bonds between C-H will break, and the carbon atoms will form a layer structure along with the other functional groups.(64)

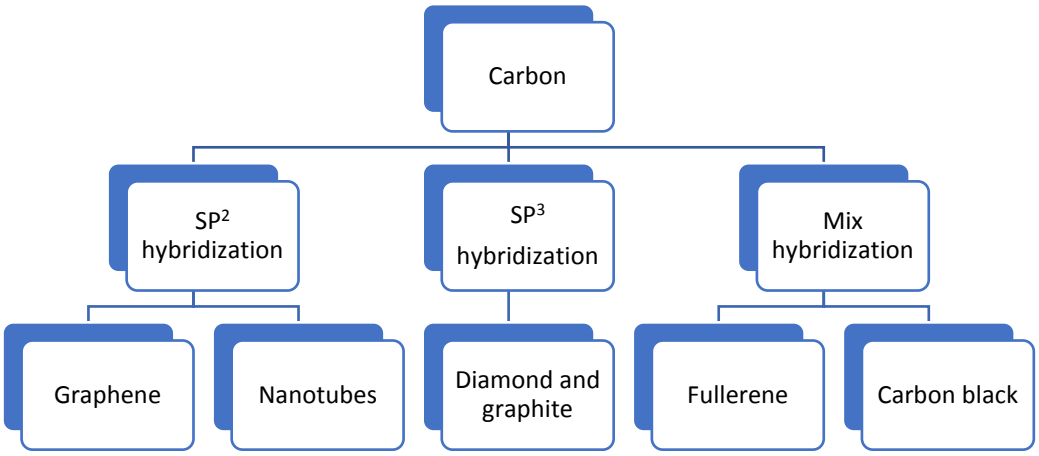

Figure 3.1 Schematic flow diagram narrating classification of the carbon materials by the type of the atomic hybridisation.

Different types of CB are available in the market, which differs in the physical characteristics, crystallinity, and composition.(65) Rubber, paint and the tyre industry are the leading consumers of the CB, but recently researchers have also utilised them as electro-active materials in super-capacitors, lithium-ion batteries, sodium-ion batteries, and sensors.(66)

3.2 Morphology of Carbon Black:

The morphology of the carbon black depends upon the type of material and method used in its production.(63) With an extensive characterisation, McCunney(67) has concluded that the CB is composed of the agglomerate and aggregates of the carbon particles with the radius between 100 nm to few microns (detail of the structure is illustrated in **Figure 3.2**).

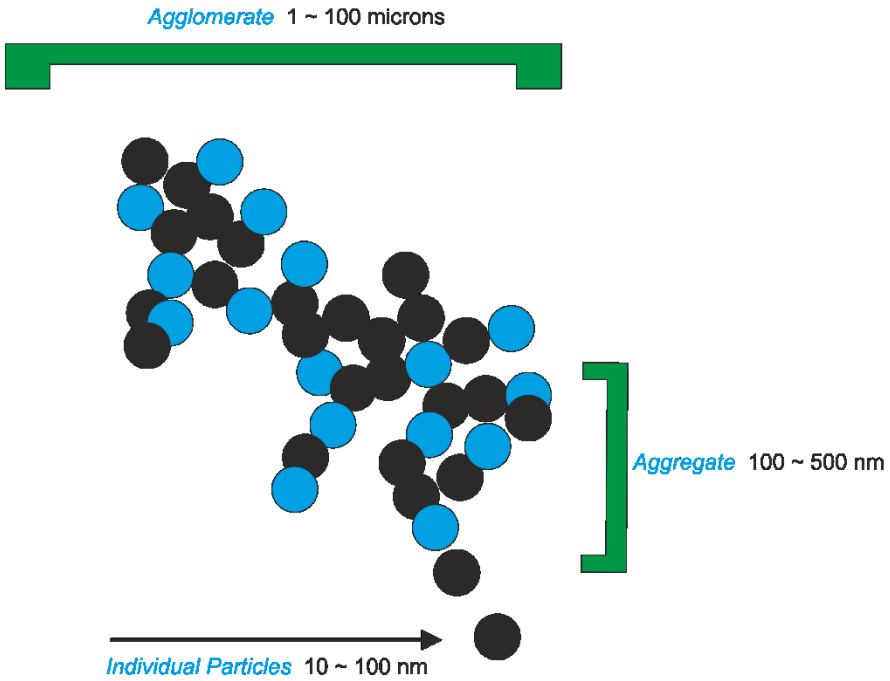

Figure 3.2 Structure of bulk carbon black which consists of the agglomerate, aggregate, and individual particles.

3.3 Carbon black composite with polymers:

The CB can be combined with a polymer to give the high strength, stiffness, wear resistance, and the electrical conductivity.(68) The CB is usually melt-blended with the polymer to achieve better dispersion.(68) The percolation threshold in CB polymeric composites is the function of the interaction between carbon black and polymer, polymer melt viscosity and its crystallinity.(69) If the interaction between the filler particles is high, then it will be difficult to obtain a proper dispersion. Similarly, if the interactive forces between the polymer and filler particles are dominating, then the polymer will encapsulate these particles.(70) Miyasaka(71) found that the percolation threshold increases with the increase of the polymer surface tension. The conductive filler particles get dispersed homogeneously in the amorphous polymer. Sumita(72) reported that the percolation threshold increases with the increase in polymer molecular weight. The conductivity of the CPC can be increased by blending with another polymer having less interaction with the filler. These particles then get concentrated in one phase which will increase the number of contacts between them.(69, 73)

3.4 Factors effecting the Conductivity of Carbon Black filled Polymeric Composites

The filler dispersion characteristics have a pronounced effect on the mechanical and electrical properties of the composite.(74) The extrusion is a primary process for dispersing a filler in a polymeric matrix.(54, 75) During extrusion, the shear is produced by the mechanical motion of a screw causing the aggregate to break down into smaller particles.(75) The compounding machines which provides more shearing forces are useful for adequate mixing and distribution of the particles.(76) The internal batch mixer, extruder, twin-roll milling, and dry mixer are the most effective compounding machines for producing the particulate filled polymeric composites.(77) Bigg(78) explored the effect of processing time and CB structure on the conductivity of the composite. Bigg studied three different CPC based on the acetylene, medium porosity Vulcan XC-72, and highly porous CB. Bigg also studied the CPC composed of the various polymers such as Acrylonitrile Styrene Butadiene (ABS), polycarbonate (PC) and polypropylene (PP). According to the study, the conductivity of the CB composites was less affected by the processing time. Among all polymers, the PP composites were found to be more conductive, and the PC composites showed the least conductivity. Bayer(79) explored the association between injection moulding and CB dispersion in polyethene (PE). Bayer found that random distribution of the CB gives the higher conductivity at low percolation threshold. Bayer also reported that the percolation threshold found to be low when the composite is produced by compression moulding. The conductivity of the CPC depends on

- The type of polymer and its properties
- Processing parameters and machines
- The nature and morphology of the filler particles

The 3D printing of the conductive polymeric composite based ECA is not similar to that of the pure polymers.(25) At present, 3D printers available in the market are only designed for linear polymers such as Polylactic acid, Acrylonitrile butadiene styrene, Polypropylene, and the Polyether ether ketone.(26) The production of CPC filament with the properties suitable for the 3D printer's feeding system requires much effort.(25)

4. Thermoplastics Composites and their properties:

The thermoplastics (TP) are widely being used because of ease of their production.(80) The TP can be processed using the blow moulding, injection moulding, centrifugal moulding, and thermoforming.(81) The CPC based on the thermoplastic requires the addition of the conductive filler which can also change its other physical properties.(82) The printing process in FDM 3D printers are designed and calibrated on the physical properties of the polymer.(83)

4.1.1 Specific Density:

The composite density can easily be calculated using general rules of mixtures(84) and is given by

$$\rho_c = \frac{\rho_f \rho_P}{\rho_P m_f + \rho_f (1 - m_f)} \quad (4.1)$$

Whereas

ρ_f is the density of a filler.

ρ_P is the density of a polymer.

m_f is the mass of a filler.

ρ_c is the density of a composite.

With the increase in the crystallinity of the polymer, the composite density will increase because crystalline grains occupy less volume as compared to the amorphous region.(85) The entrapped air caused by the improper mixing can also increase the density of the composite.(85)

4.1.2 Melt Viscosity (MFI)

The fluidity of the polymer melt is related to its viscosity, melt flow rate and the melt viscosity index (MVI).(86) It can be evaluated by a simple experiment in which the pressure is applied to the melted polymer to pass an orifice. The measured value of the polymer mass in grams passed through a hole in a specific time is its MVI and is the inverse of the viscosity.(87)

4.1.3 Volume output

The extruders are mainly used as the mixing equipment for compounding the particulate composite.(88) The efficiency of the operating procedure is related to the output of the compounding machines. It can be expressed as the mass or volume coming out in a unit time.(84)

4.1.4 Thermal Conductivity and Specific Heat Capacity

The thermal conductivity of the polymer blend defines its rate of cooling or heating.(89) In the processing of TP, a melted liquid is moulded in the desired shape.(90) The polymer with higher thermal conductivity can be melted quickly which directly increases the production rate. When the polymer is filled with conductive additives, their thermal conductivity will increase.(91, 92)

4.1.5 Thermal Expansion

The thermal expansion coefficient (TEC) of the material defines the degree of change in the physical dimensions when subjected to heat.(93) The metal, ceramics, and polymers have different values of TEC.(94) The polymer expands excessively upon heating as compared with other additives in a composite.(85) The TEC for the polymer is much higher than the mineral fillers and metals. When the polymer is blended with the conductive filler, the TEC will change accordingly.(95)

In FDM, the process flow is controlled by the above-explained physical properties of a plastic.(25, 26) The CPC based filaments have different properties than their counter polymeric bulk filaments. At present, we have commercially available FDM printers which are designed for pure polymers. The rapid integration of the composite filament with these printers needs the attention of the research and industrial community.(96)

5. Polymer Processing

The polymer compounding refers to the set of all processes which are utilised to convert polymer into the desired product.(97) The process selection for the compounding depends on the characteristics of polymers and additives. The designing and selecting the efficient compounding process is necessary to obtain a well dispersed and homogeneous composite.(98)

5.1 Feedstock transportation:

The nature of the feedstock influences its handling and the speed to which it can be transported to the compounding machine.(97) The polymers and additives are in the granule form of different shape and size.(99) The feedstock transportation of the polymer and particulate additives depends upon their affinity to water absorption, the tendency toward deformation under the pressure and ability to agglomerate by surface attraction.(100) The filler which can absorb water through the atmosphere will need drying before adding it in a matrix. The particles which can face rupture due to shear forces need to add slowly in the massive compounding machines.(101)

5.2 Melting:

During the compounding, the heat required for the fusion can come from many different sources, i.e., the thermal conduction, the frictional forces between particles, and the mechanical forces produced during mixing.(102) The melting of the polymer by thermal conductance from the surrounding metal will need more energy because polymers have low thermal conductivity. The polymer shearing gives a uniform and efficient heating but also can cause decomposition of the polymer.(97) Therefore, the melting chambers are designed by considering the multiple sources of the energy. The speed of the melting depends upon many different factors and is related to the type of the polymer and additives.(103)

5.3 Melt mixing:

The adequate blending is essential to obtain homogeneous properties of the composite.(97) During mixing, the filler undergoes to the following stages(85).

- The melted polymer encapsulates the filler particles.
- The breakdown of the agglomerate of the filler particles.
- The distribution of the agglomerate into the polymer.

These stages for the different materials not necessarily depending on the same factors. For example, the breakdown of Titania agglomerates is caused by erosion, whereas the CB dispersion occurs by rupture.(104) Many attempts have been made to measure the forces occurring on the particles during dispersion. The most accurate formulation can be obtained by considering the rigid dumb-bell shaped single agglomerate having different beads with

radius r_1 and r_2 which are connected. Suppose this system is in a homogeneous velocity field of an incompressible Newtonian fluid. The maximum force between the beads occurring at the angle of 45° between shear direction and dumbbell orientation is given by(105)

$$f_{max} = 3\pi\eta\gamma[\frac{r_1.r_2}{r_1 + r_2}]L \quad (5.1)$$

Where η is the viscosity of the melted fluid, γ is the shear force, and L is the length of the joining beads. Now, consider that the dumbbell is moving in the flow direction, then the maximum separating force can be expressed as(105)

$$f_{max} = 6\pi\eta\varepsilon[\frac{r_1.r_2}{r_1 + r_2}]L \quad (5.2)$$

It is evident from the above equation that the larger agglomerates are more easy to break down than the smaller one.

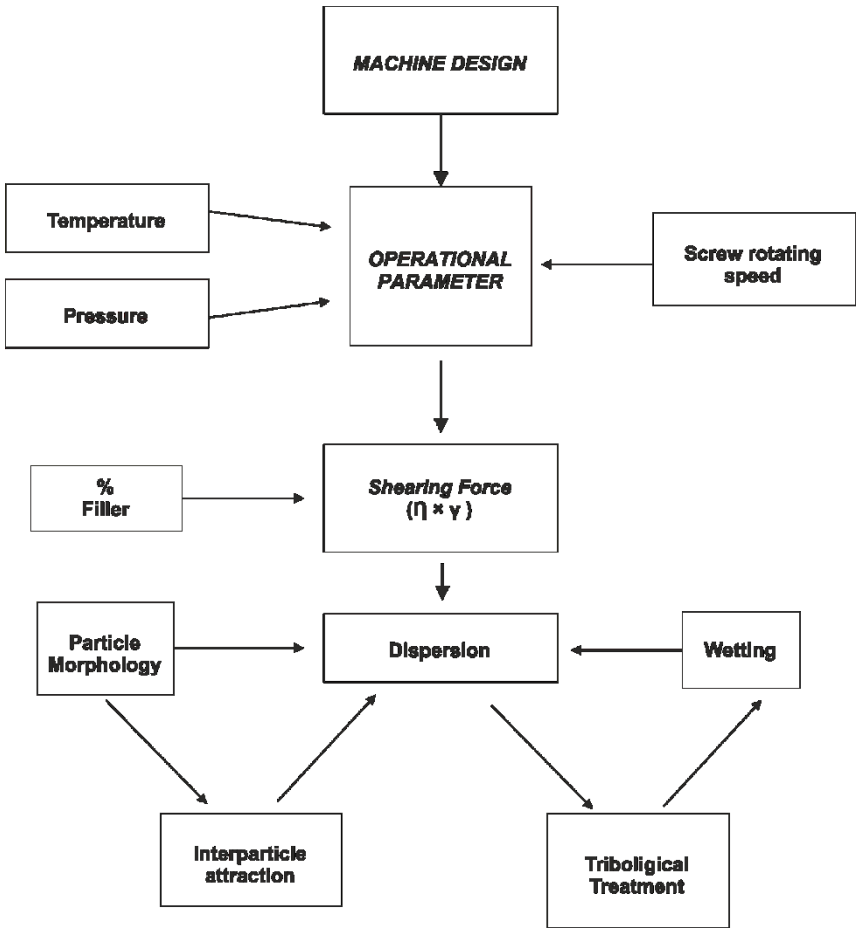

Figure 5.1 Summary of the factors affecting the dispersion of the filler in a polymeric matrix. Reproduced from (84)

5.4 Devolatilisation:

The devolatilisation is a process of removing the volatile materials from the feedstock.(97)The volatile materials mainly include the adsorb moisture content and the unreacted monomers which can affect the final properties of the composite.(85, 97) In open bed compounding processes, the pre-devolatilisation is not required, and volatile material can escape from the polymer bed and hopper. However, the devolatilization of the feedstock is essential for the closed bed designed compounders such as twin screw extruders.(106)

5.5 Melt pressurisation:

Maintaining the sufficient pressure of the polymer melt is essential to convey the mass for efficient production.(97) The addition of the particulate fillers increases the viscosity of the melt, which subsequently increases the minimum pressure required for the smooth flow. The excessive pressure is usually applied to assure proper feeding of a melt to the narrow channels.(107)

In conclusion, the composite manufacturing is a multistep procedure, and the optimal condition for producing the polymeric composite depends upon the characteristics of its constituents. In FDM, the polymer filament is used for printing which was already produced by using a compounding process. In future, the 3D printers capable of directly converting the feedstock to the desired product can also be realised. However, much effort is required to integrate the compounding processes with the additive manufacturing.

6. Interpreting Electrochemistry:

6.1 Electrochemistry

The electrochemistry is an integrated domain of the basic chemistry and physics, which has proven to be cardinal in the plethora of recent technological advancements.(108) It is the study concerning the electron transfer between the electrode surface and the interfacial electroactive species.(109) The electrochemical techniques are based on measuring the current by varying potential of the electrode or vice versa, which directly or injection with the other scientific relations can be expressed as valuable information.(110)

6.2 The electrode potential:

The metallic atoms organise themselves in a regular array known as the crystal structure. This specific arrangement of atoms gives birth to the orbital bands, and each band is associated with the set of physical parameters.(111) When a metallic material is placed in an electrolyte, depending upon the potential at the surface, the ions (negative or positive) will migrate toward it. Thus, creating the polarised interfacial region which is also known as an electrochemical double layer.(112) Next, to the double layer, there exists a diffusion region where ionic species can move without the influence of the external forces (as illustrated in **Figure 6.1**).(112) Here, the potential has already been established between the surface and electrolyte interface. However, the potential of the solid/liquid junction cannot be measured without connecting it to the reference electrode.(113) The reference electrode (RE) exhibits a stable potential whose value is known and is used to calibrate the potential of the working electrode (WE).(114)

6.3 Electroanalytical Methods:

Electroanalysis is the fundamental technique in the plethora of the modern analytical technology.(108) Consider a piece of the metal as a WE and is connected to the counter electrode for completing the circuit in the electrolyte. The potential of the electrode can be changed by connecting CE and WE with an external source of electricity. To control/measure the potential, WE is connected to the reference electrode (RE). The three-electrode system immersed in the electrolyte represent a hierarchy of electroanalytical technique as shown in **Figure 6.1**.(115)

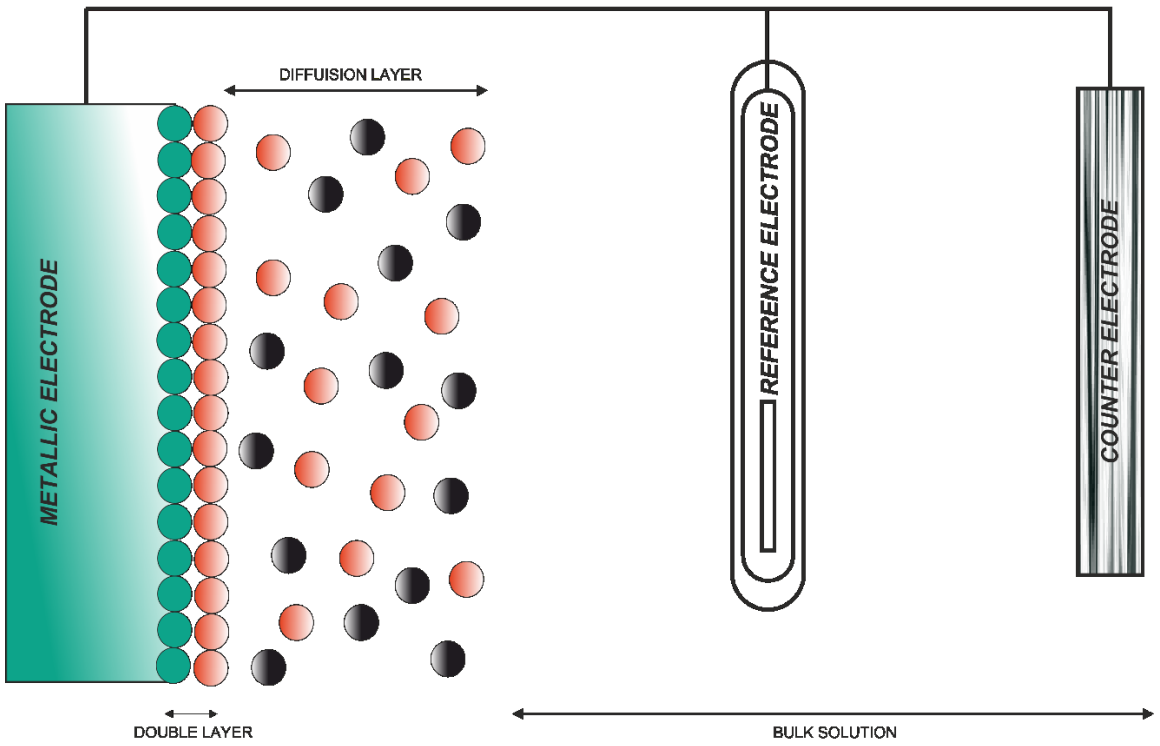

Figure 6.1 Illustration of the three electrode electroanalytical process highlighting double and duffusion layer when electrodes are subjected to change in a potential.

The electrical instrument along with the computer software is used to measure and control the potential/current of the electrochemical circuit. The electroanalytical methods are usually classified into the two primary classes, i.e., the potentiostatic and potentiometric.(109) If the

reversible reaction is occurring at the WE surface in which O_x and R_x represent the oxidised and reduced ionic species respectively, then the reaction can be expressed as

$$O_x + ne^- \underset{\leftarrow}{\rightarrow} R_x \quad (6.1)$$

The reaction involves the transfer of charge from the electrode to the electrolytic ions, and the work done (W) will be equal to the product of the charge (Q) and the potential (E).(116)

$$\mathrm{W} = \mathrm{QE} \quad (6.2)$$

Whereas, the charge produced from the one mole (n) of the electron transfer can be expressed as,

$$\mathrm{Q} = \mathrm{nF} \quad (6.3)$$

Whereas, F is a Faraday Constant. By combining the equation 6.2 and 6.3

$$\mathrm{W} = \mathrm{nFE} \quad (6.4)$$

The work done is equal to the change in the free energy (ΔG), and the above equation can be expressed as

$$\Delta\mathrm{G} = \mathrm{nFE} \quad (6.5)$$

According to the law of thermodynamics, the free energy change during the chemical reaction can be expressed as(116)

$$\Delta\mathrm{G} = \Delta\mathrm{G}^\circ + \mathrm{RT}\ln Q \quad (6.6)$$

$$-\mathrm{nFE} = -\mathrm{nFE}^\circ + \mathrm{RT}\ln Q \quad (6.7)$$

$$\Delta\mathrm{G} = \mathrm{nFE} \quad (6.8)$$

$$\mathrm{E} = \mathrm{E}^\circ - \frac{\mathrm{RT}\ln Q}{nF} \quad (6.9)$$

Whereas the R is the universal gas constant, T is the temperature and Q is the ratio of the concentration of reduced and oxidised ions. By substituting the values of the constants, the equation can be delivered as

$$\mathrm{E} = \mathrm{E}^{\circ} - \frac{0.059}{n} \ln Q \tag{6.10}$$

In a forward reaction, the Nernst equation becomes

$$\mathrm{E} = \mathrm{E}^{\circ} - \frac{0.059}{n} \ln \frac{[R_x]}{[O_x]} \tag{6.11}$$

The above equation is known as the Nernst equation, which relates the potential and the concentration of the ions.(116) If the controlled potential is applied between WE and CE, which are immersed in the electrolyte containing the electroactive species such as hexa-mine-ruthenium (iii) chloride. The electroactive species can approach the solid surface by three different schemes, i.e. migration, diffusion, and convention. The oxidation-reduction of the ions approaching the electrode will occur at the potential where the electron transfer becomes thermodynamically favourable.(115, 117, 118) The current is the measure of the flow of charged particles in the solution. Thus, the current generated because of the applied potential depends upon multiple factors, i.e., the electrode and analyte characteristic, potential sweep rate, etc.(118) This potential-current relation from a reaction can be utilised to probe the characteristics of the electrode or the analyte.(118) The classification of the electro-analytical techniques is elaborated in **Figure 6.2**.

6.4 Cyclic voltammetry:

The electro-analytical technique based on the signal derived through the charge transfer reaction can be classified into two main groups, i.e., the potentiometry and amperometry. In potentiometry, the potential between the electrodes is measured as the function of the applied current (static electro-analysis, I = 0). Whereas, the amperometry is a measure of the current by subjecting a potential range between the electrodes (dynamic electro-analysis, I ≠ 0).(119) The cyclic voltammetry (CV) is the widely being used technique in which the cyclic

potential is applied to the three electrode system, and the resultant current is measured as a function of the subjected potential.(120)

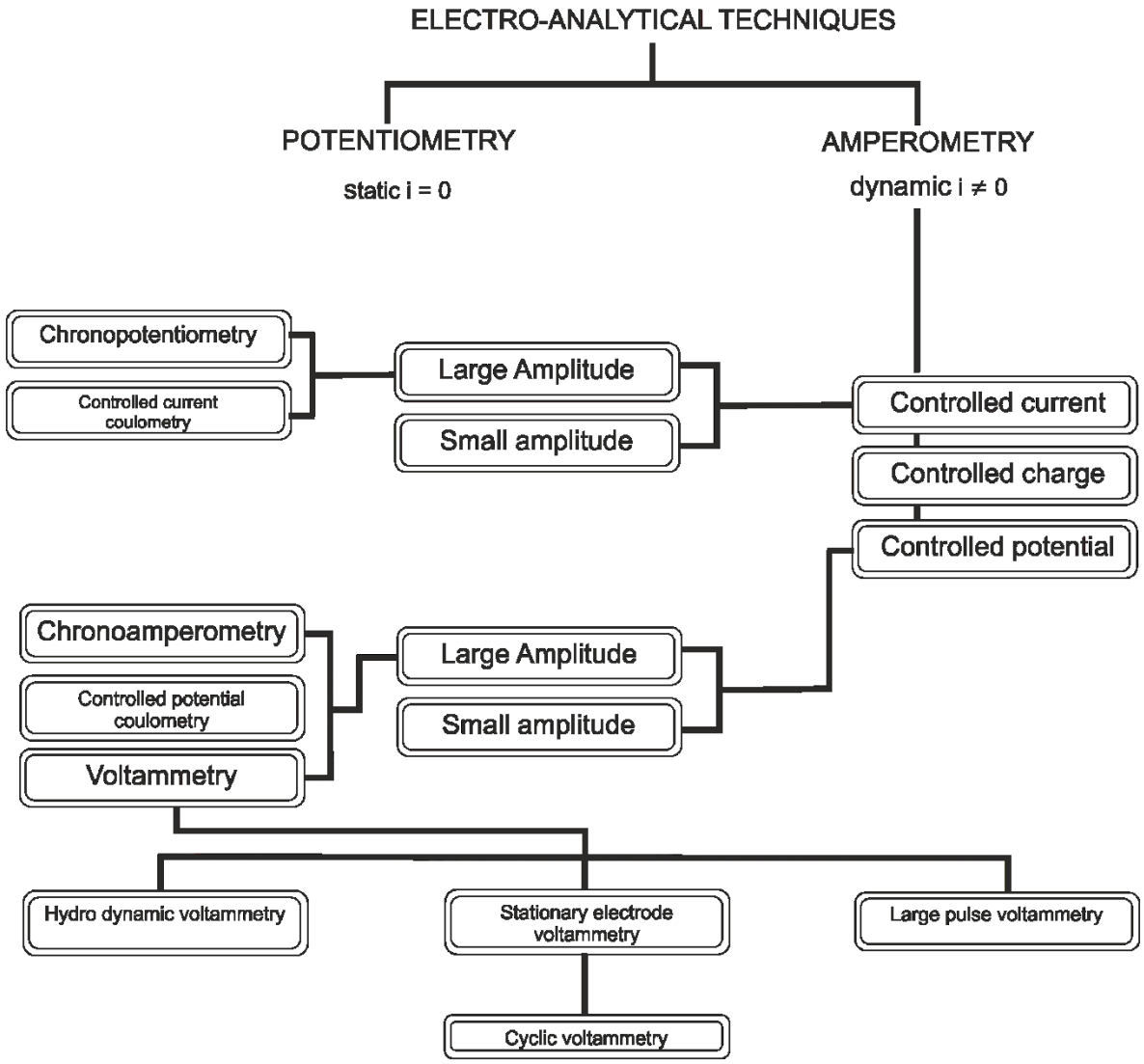

Figure 6.2 Flow sheet elaborating the classification of the electro-analytical techniques Reproduced from reference(121)

In cyclic voltammetry, the potential is changed from V_1 to V_2, and then again reversed from V_2 to V_1. The applied sinusoidal potential signal and the recorded current is depicted in **Figure 6.3** (C). The rate at which the potential V_1 to V_2 is swept is known as the scan rate and is measured as volts per second (V/s). When the potential is applied across the electrode, the surface concentration changes as defined by the Nernst equation.(122) The vicinity between the working electrode and the bulk solution known as diffusion layer will face the deficiency of the reactant. The ions from the bulk solution will move toward the diffusion layer for

maintaining the neutrality of the charge and is a measure of the current.(120) According to the Fick's law of the diffusion

$$J(x,t) = D\ \frac{dC(x,t)}{dx} \tag{6.12}$$

Where, C, x and t are the concentration of an analyte, distance (position) and time respectively. The magnitude of the current is the function of the rate of reaction occurring at the electrode.(122) The ions are not approaching the electrode by a single mechanism, i.e., diffusion is not the only process behind the mass transport. In this situation, Fick's law of diffusion cannot be used to calculate the produced current.(122) The Nernst-Plank equation is used to calculate the flux governed by multiple processes and mathematically can be given as

$$J(x,t) = -D\left[\frac{dC(x,t)}{dt}\right] - \left[\frac{zFDC(x,t)}{RT}\right]\left[\frac{d\phi(x,t)}{dx}\right] + C(x,t)V(x,t) \tag{6.13}$$

Where z, F, $\frac{C(x,t)}{dt}$ and V(x, t) are the charge, Faraday's constant, concentration gradient (at distance x and time t) and the drift velocity of the ions respectively.(123) The current (I) produced by the electrochemical reaction is directly proportional to the flux and can be given as

$$I = nFAJ \tag{6.14}$$

The electroanalytical methods based on the potential sweep such as cyclic voltammetry probes the effects of change in potential in relation to the monitored current.

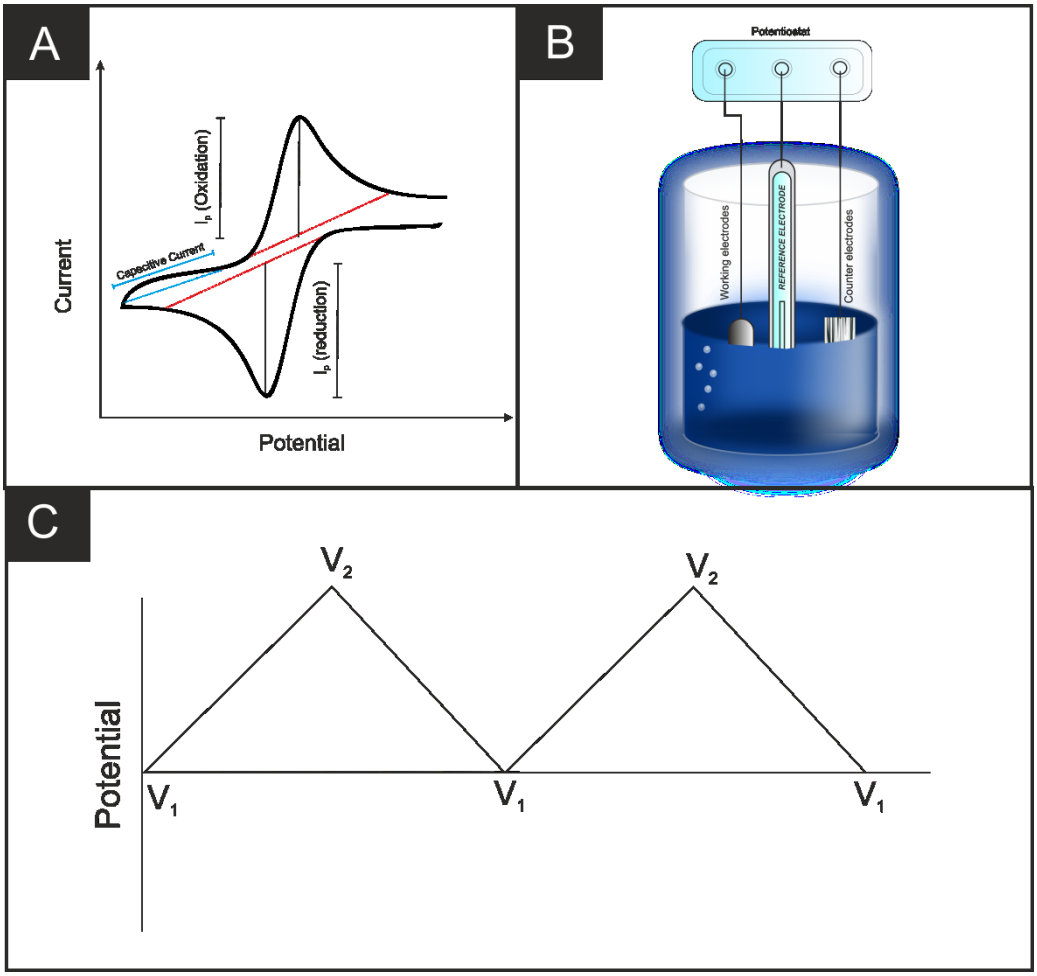

Figure 6.3 (A) The graphical representation of the data fetched from the cyclic voltametry experiments along with the certain percieved parameters. (B) the schematic illustration of the three electrode system for conducting cyclic voltametry experiments. (C) the potential sweep wave during the experiment.

7. Results and Discussion:

7.1 Methods

7.1.1 Materials:

The Carbon black (Super P® Conductive, 99+ %), and the Graphene nanoplatelets (GN) were obtained from the Alfa Aesar (UK), and the Graphene Supermarket (USA) respectively. The Acrylonitrile butadiene styrene (ABS), and the Polylactic acid (PLA) pellets were commercially procured from Sabic (UK). The melt mixing technique was used to prepare the polymer blend of the acrylonitrile butadiene styrene and the recycled polycarbonate (ABS-PC). O-xylene, potassium chloride, hexaamine-ruthenium(iii) chloride, and nano-graphite mesoporous (500 nm) were purchased from Sigma Aldrich (UK). All chemicals were of analytical grades and were used without any purification. All solutions were prepared using the deionised water with the resistivity not less than 18.2 MΩ cm.

7.1.2 Recycled polycarbonate blending with Acrylonitrile butadiene styrene:

The waste gadget of the polycarbonate was crushed into pellets using the pelletizer. Then this polymer was melt-blended with ABS using the twin screw HAAKE™ Rheomix OS Lab Mixer (ThermoFisher, United Kingdom). The temperature of the both plates was kept at 215 °C, while the speed of the screws was adjusted at 70 rpm. After 10 minutes of the mixing, the prepared polymer blend was taken out from the melt chamber followed by the cooling under ambient conditions. Finally, this polymeric blend was turned into pellets using the pelletizer.

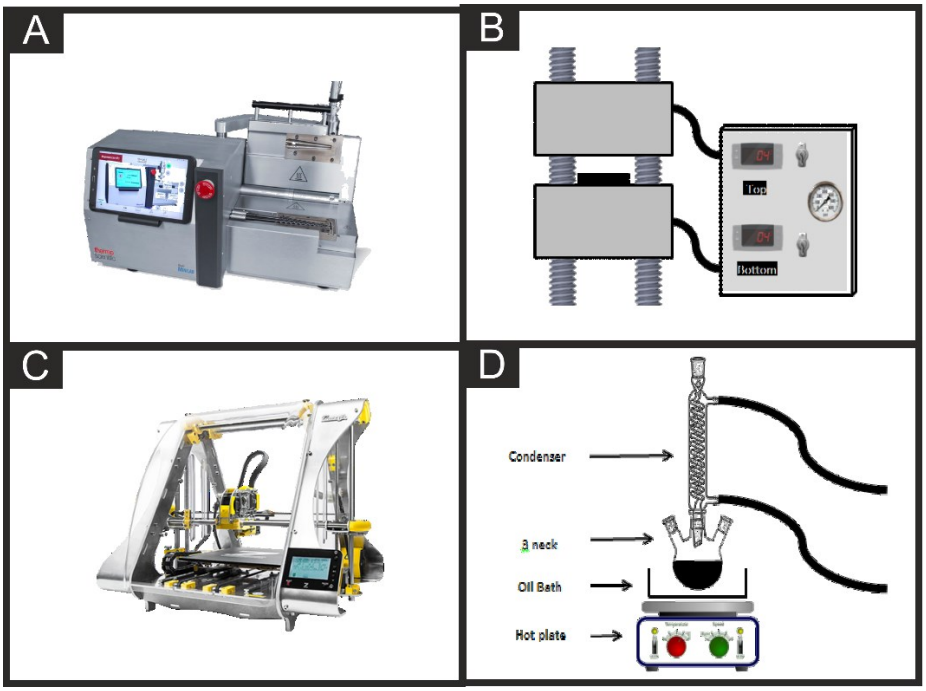

Figure 7.1 (A) Thermofisher mini compounder, (B) the illustration of the hot press used for the production of TF, (C) Z-morp 3D printer, and (D) demostrating the process of blending through solution mixing. Reproduced from Ref (124, 125)

7.1.3 Polymer blending with filler:

The polymer mixing with the filler was achieved by using the solution-mixing technique. For this, the filler particles of the required amount were dispersed in 100 ml of o-xylene and sonicated for 2 minutes. Then, this dispersion was transferred to a three-neck round bottom flask and heated to 120 ° C, while stirring it at 400 rpm using a magnetic stirrer. When the temperature reached 120 °C, then it was left for another 40 minutes followed by adding a required amount of the polymer pellets into the solution. After 4 hours of mixing, the produced mixture was inverted to a beaker and cooled down by stirring it under the ambient conditions. Upon cooling, 150 ml of the methanol was added while stirring it continuously. This solution was filtered and washed with the 250 ml of methanol. Obtained polymeric blend then dried in an oven at 50 °C for 24 hours. The amount of the filler and polymer used for different batches are listed below in **Table 7.1**.

Table 7.1 List of the amount of the filler and polymer used for different batches for producing the composite.

Filler percentage (mass %)	*Mass of polymer* (grams)	*Mass of Carbon black* (grams)
20	4	1
18	4.1	0.9
16	4.2	0.8
15	4.25	0.75
14	4.3	0.7
12	4.4	0.6

7.1.4 Filament Production:

The filament (for manufacturing the 3D printed electrochemical architectures) was produced using the HAAKE Minilab micro twin screw compounder (ThermoFisher, United Kingdom). The mixing chamber was preheated to 180 °C, followed by adding 5 grams of the composite powder produced by solution mixing. The speed of the screws was kept to 35 rpm throughout the operation, and after 9 minutes of mixing, the melted polymer blend was forged through a hole to get a filament with a required diameter.

7.1.5 3D printed electrodes

The 3-dimensionally printed electrodes (3DE) were fabricated using FDM based Z-morph 2 SX 3D printer (Wroclaw, Poland). The filament was inserted into the (3D printer's) extruder which was operated at 210 °C and electrodes were fabricated to the required dimensions (as shown in **Figure 7.2**). The computer-aided design of the 3D printed electrodes was generated using the Solidworks.

7.1.6 Thin film production:

For the manufacturing of the Super P carbon black based polymeric thin films (TF), two Teflon sheets (RS Components, UK) with the 10 cm^2 of the area and 1.5 mm of the thickness were used. These sheets were placed in the centre of the metallic plates followed by preheating it for two minutes at 230 °C using hydraulic hot press (Bradley and Turton Ltd, Kidderminster, Worcestershire, United Kingdom) under 1500 tons of pressure. The wrought iron metallic plates with the rectangular area of 1.5 ft^2 and thickness of 1 cm were used. After the metal plates were removed, approximately 1 gram of a polymeric blend powder was dispersed using a stainless-steel spatula over a small area between the Teflon sheets. These sheets were then heated again to 230 °C for 2 minutes using hot press under 1500 tons of pressure. Finally, these plates were transferred to a hydraulic cold press fitted with water cooled platens (15 °C) (Francis Shaw and Company limited, Manchester, United Kingdom) to cool it down under 400 tons of pressure. The produced TF were separated out and cut with a scissors to the appropriate size (as shown in **Figure 7.2**) for the electrochemical testing.

7.1.7 Cyclic voltammetry study:

The voltammetric study was conducted by using the three-electrode system with the Autolab PGSTAT101 potentiostat (Metrohm, Netherland). Whereas the platinum wire and saturated calomel electrode were used as the counter and reference electrode respectively. The thin film (with a rectangular area of 0.7 cm^2) and 3DE (with a circular area of 0.071 cm^2) was used as working electrodes. Whereas hexaammine-ruthenium(III) chloride was used as a redox probe, and the solution of 1mM hexaammine-ruthenium(III) chloride/ 0.1M Potassium chloride was degassed with nitrogen for 10 minutes before running the experiments. All the experiments were conducted under the ambient conditions. The edge plane pyrolytic graphite electrode (EPPG) was produced from the highest available grade (SPI-1) of highly oriented pyrolytic graphite (Le Carbone Ltd, United Kingdom) having the Lateral grain size of 1-10 µ and 0.4 ± 0.1° mosaic spread. The EPPG electrode were produced by machining the highly oriented pyrolytic graphite (HOPG) along the direction of the edge plane into the cylindrical shape with diameter of 4.9 mm. The complete production process of EPPG and its characterisation was previously discussed and reported (126). The screen-printed electrode was fabricated using the microDEK 1760RS screen printing machine (DEK, Weymouth, United Kingdom) and the suitable stencil designs to achieve the 3 mm diameter of the working

electrode. The graphite ink (Product Code: C200802P2; Gwent Electronic Materials Ltd, United Kingdom) was first printed onto the flexible polyester sheets of 250-micron thickness (Autostat, Milan, Italy) and cured in the vaccum oven at 60 °C for 30 minutes. The dielectric paste (Product Code: C2000802P2; Gwent Electronic Materials Ltd., United Kingdom) layer was then printed over the cured graphite ink to cover the connections.

7.2 Results and discussion

The Fourier transform infrared spectroscopic analysis were conducted with the Perkin Elmer Spectrum Two FT-IR Spectrometer under the ambient conditions using infrared rays of wavenumber between 450 to 4000 cm^{-1} with the minimum of the 4 scans at a resolution of the 1 cm^{-1}. The Perkin Elmer spectrum 10 software was used to record and analyze the data of the FTIR experiments. The peaks within the range of 3000–2800 cm^{-1} and 1365 cm^{-1} in FTIR spectra showed that the stretching and bending of the aliphatic bond of ABS between carbon and hydrogen (C—H) respectively.(127) The stretching vibration of the aromatic C—H bond appeared at 3200–3000 cm^{-1}. The absorption at 2237 cm^{-1} was related to acrylonitrile group. The peak at 1602 cm^{-1} identified the stretching vibration of the carbon-carbon double bond of the butadiene.(127) The absorption at 1474 cm^{-1} was from the stretching vibration of the aromatic ring of styrene. The hydrogen-bonded alkenic carbons from 1,2 butadiene and 1,4 butadiene showed absorption at 910 cm^{-1} and 966 cm^{-1} respectively. Other than the all above identify absorptions, the polycarbonate molecule showed the characteristic peaks of carbon-oxygen bond around 1200 cm^{-1}, while of carbonyl and methyl group are at near 1772 cm^{-1} and 2800-3000 cm^{-1} respectively. The peaks at 911 cm^{-1}, 967 cm^{-1}, 2237 cm^{-1}, and 1772 cm^{-1} showed that the ABS and PC were the constituents of the blend.(127, 128) The peaks at near 3500 cm^{-1}, 1750 cm^{-1}, and 1449 cm^{-1} were due to hydroxyls, carboxylic and methyl groups of PLA.(128, 129) The shifts of the characteristic peaks of the PLA polymeric composites were observed toward lower wave number as compared to the standard pure polymeric material. The hydroxyl, carboxylic and methyl groups peaks of the 15% SP blend with PLA appeared at 3351 cm^{-1}, 1748 cm^{-1}, and 1442 cm^{-1} respectively. The peaks of the hydroxyl groups were more shifted from the standard value. However, the FTIR peaks of other groups of the PLA molecule were not significantly shifted as compared to the hydroxyl group which lies on the end of the polymeric chains. Mofokeng(130) along with co-workers reported a similar trend for the PLA composites with natural fibers and they proposed that this shift was because of

free hydroxyl groups were engaged in hydrogen bonding. In contrast, the characteristics peaks of the ABS and PC not showed any appreciable shifts with the additions of the filler particles in it. The relative data of the peaks position of the constituent molecular groups of the PLA composites are given in **Table 7.1**. The peak broadening and the shift in the absorbance wavelength of the polymer characteristic peaks is associated with the interaction between the filler and the matrix.(131) The harmonic oscillation model for the reduction in the force constant can be given as(132)

$$\boldsymbol{\Delta} f = f_{nb} - f_b = \frac{\boldsymbol{\mu}(\boldsymbol{v_{nb}} + \boldsymbol{v_{nb}})}{4\pi^2} \quad (7.1)$$

Where v is the oscillation frequency, f is a force constant with the subscript nb and b denoting the non-bonded and bonded oscillator. Where $\mu = m_1m_2/(m_1 + m_2)$ is the reduced mass of the oscillation. The force constant of the covalently bonded atoms is directly proportional to their mass m_1 and m_2 and frequency of the oscillation between them. The force constant of bonds between the atoms of the polymer molecular can be reduced by some interaction with filler particles and is directly proportional to the shift in the vibration of the atoms.(131, 132) The lowering of the peak frequency associated with the interaction (physical or chemical bonding) between the filler particles and polymeric molecules.(131) The obtained FTIR spectra for ABS-PC and PLA specimens are graphically represented in **Figure 7.5** and **Figure 7.6** respectively.

Table 7.2 List of the FTIR peaks positions of the constituent molecular groups of the PLA composites.

SAMPLE	WAVE NUMBER (cm^{-1})		
	HYDROXYL	CARBONYLE	METHYLE
PURE PLA	3500	1750	1449
15% SP/ PLA	3351	1748	1452
20% SP/ PLA	3347	1740	1445
25% SP/ PLA	3335	1746	1453
15% GRAPHENE/PLA	3422	1747	1448

20% GRAPHENE/PLA	3353	1744	1448
25% GRAPHENE/PLA	3335	1738	1444
15% NG / PLA	3362	1741	1447
20% NG/ PLA	3364	1743	1442
25% NG/ PLA	3343	1747	1445
20% F(50% SP – 50% GRAPHENE)/PLA	3381	1740	1447
15% F(50% SP - 50% GRAPHENE)/PLA	3383	1745	1447
15% F(50%NG - 50% GRAPHENE)/ PLA	3348	1745	1450
20% F(50%NG – 50% GRAPHENE)/ PLA	3336	1742	1449

Recently, the 3D printing has drawn much attention in direct writing of a structure for the electrochemical applications.(133) The ink-based 3D printers have expanded the range of the material to be printed three-dimensionally. However, the produced structure requires the post-treatment (such as nitrogen freezing, freeze drying, and heat treatment) to give strength, conductivity and porosity.(134) Recently, Pumera(135) proved the gold plated-metal 3D printed electrodes as a promising alternative to the glassy carbon. The fabricated metallic 3D printed ECA were found to be more sensitive toward phenol and p-aminophenol as compared to the glassy carbon. However, the implementation of these gold-plated surface was limited by the formation of the organic films and the molecules with higher oxidative potential cannot be detected accurately.(135) Banks(136) along with his co-workers were first to examine the electrochemistry of the polymer-based 3D printed electrodes (3DEs). They printed the 3DEs of commercially available graphene-based plastic filament using RepRap FDM printer and studied their electrochemical response. They tested the 3D tailored ECA of

polylactic acid (PLA) filled with graphene in solid-state super-capacitor, lithium-ion battery and hydrogen evolution reaction. However, they showed a minute efficiency due to the low conductivity of ECA.(136) The graphene as a filler particle was encapsulated by the insulative polymer providing a low electroactive surface interaction and consequently gave a weak electrochemical response.(136, 137) Pumera(137) also used the commercially available graphene-based filament to produce 3DE using the FDM printer. The surface of these electrodes were modified by dipping them in a polymer dissolving solvent. The surface polymer got dissolved, leaving the free-standing electro-responsive materials which aided in the improvement of the electrochemical signal.(137) However, there is no study available addressing the electrochemical response of the polymeric composite other than that of the graphene-based CPC. Moreover, there is not any published data available explaining the effect of the processing parameters on the electrochemistry of the polymeric electrodes. In this research work, the polymeric composites with different electroactive materials (other than graphene) were subjected to the electrochemical studies. Furthermore, the effect of the 3D printing on the electrochemical behaviour of the conductive polymeric composites (CPC) is discussed on the logical and experimental basis.

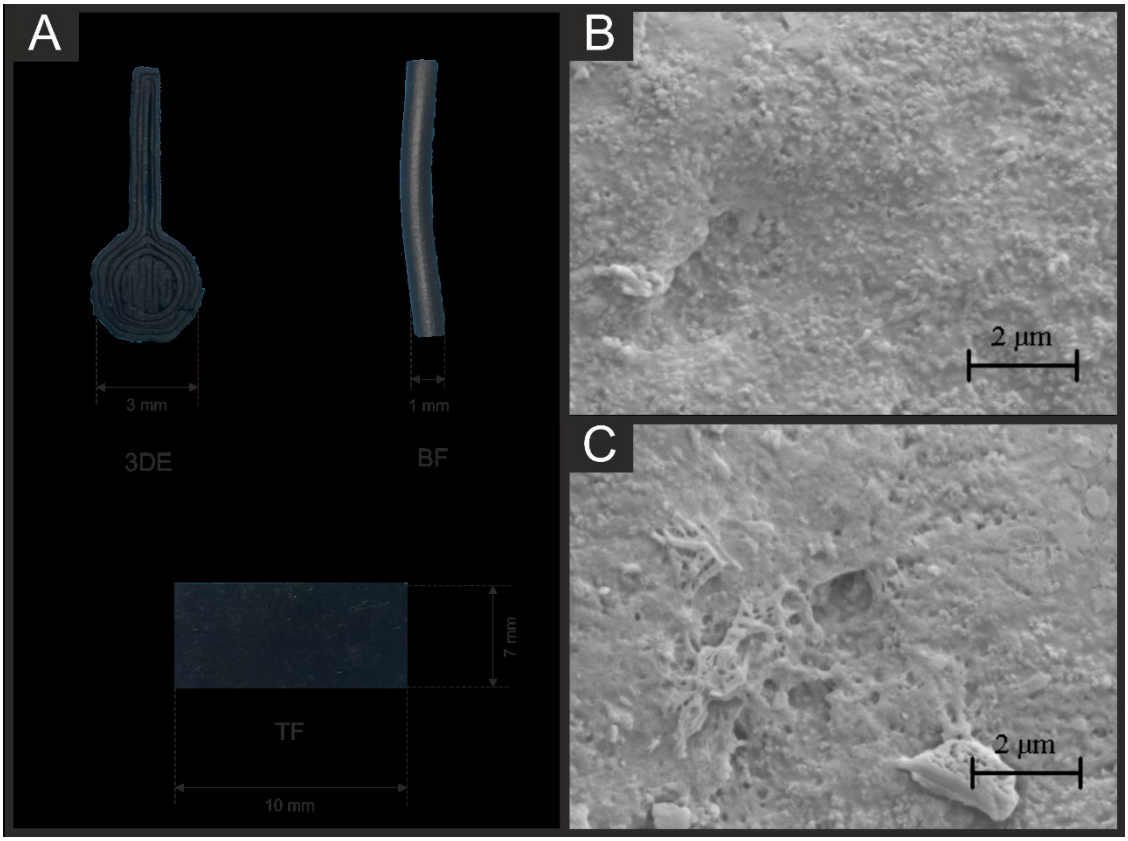

Figure 7.2 (A) TF, BF, and 3DE electrodes along with dimensions, (B)and (C) scanning electron microscopy images of the 20% graphene/PLA 3DE.

For studying the electrochemical response of the CPC, the voltammetric experiments were conducted at the range of scan rates (between 5 to 400 mVs^{-1}) using the bulk filament (BF), thin film (TF), and the 3D printed electrodes (3DE). The production method of these electrodes was already discussed in the experimental section and their relative dimensions were given in **Figure 7.2**. All the data from the voltammetric experiments is shown in **Table 7.3** to **Table 7.10**. The outer sphere probe hexaamine-ruthenium (iii) chloride was chosen as the redox probe as it was already studied in exploring the electrochemistry of the CPC electrodes.(136) The TF of the ABS and ABS-PC with a higher concentration of the Super P (Alpha Aser) showed the quasi-reversible electron transfer reaction, distinctly at slower scan rates i.e., the peak separation ($\Delta E = E_{p,c} - E_{p,a}$) was greater than 59 mV.(138)

The graph between peak current vs scan rate for 20% SP-ABS (TF), 18% SP-ABS, 20% SP-ABS-PC, and 18% SP-ABS-PC showed the gradient with the values close to 0.5 which proved that the charge transfer occurred according to the semi-infinite linear diffusion model.(139) The graph between peak current vs scan rate of CPC below 18% loading of the filler showing the

values less than 0.35 predicting the presence of the absorbs species and the charge is not only transferred by the difusional process.(120, 140) However, the overall trend showed that the peak currents were decreased by lowering the filler concentration, while peak separation increased (see **Figure 7.7**). This suggested that the filaments with higher percentage loading of the electroactive material will be helpful in increasing the efficiency of the CPC electrodes. It is a well established fact that blending a conductive filler with two immiscible polymers can enhance the conductivity, i.e. the CB composite with ABS-PC should exhibit low resistivity than its blend with the pure ABS.(141-143) With the addition of the second polymer, two situations can happen, either the filler concentration increases in the grain of the single polymer or the filler particles come on grain boundaries.(56, 141, 142, 144) When the TF of the SP composites with the ABS and ABS-PC were subjected to cyclic voltammetric experiments. The ABS pure TF showed the higher peak currents and active electrochemical area as compared with ABS-PC. The electrochemical area was calculated using the Randles Sevcik equation for the reversible systems. According to the equation, the peak current is directly proportional to the square root of the scan rate.(139)

$$I_P = (2.687 * 10^5) * \ N^{1.5} * A * D^{0.5} * [C] * v^{0.5} \quad (7.2)$$

By rearranging the equations, we get:

$$\frac{I_P}{v^{0.5}} = (2.687 * 10^5) * \ N^{1.5} * A * D^{0.5} * [C] \quad (7.3)$$

And rearrange for area (A). Where,

D = *diffusional coefficient* **(cm^2/s)**

N =*number of electron transfer*

A=*area* **(cm^2)**

[C]=*concentration* **(moles)**

$\frac{Ip}{v^{0.5}}$ = gradient of the graph between square root of scan rate (x-axis) and the peak currents (y-axis).

The electrochemical area of TF of 20% SP/ABS and 20% SP/ABS-PC were found to be 3.047 x 10^{-3} and 7.64 x 10^{-4} cm^2 respectively. The graph between peak current vs scan rate of CPC of SP/ABS and SP/ABS-PC below 18% loading of the filler showing the values less than 0.35 prediciting the presence of the absorbs species and the charge is not only transferred by the difusional process.(120, 140) In this case, the electrochemical effective area of the electrode can't be calculated using the randle sevcik equation for reversible systems. The electrochemical effective area for the 20% SP/ABS and 20% SP ABC/PC were found to be 1.11 x 10^{-3} cm^{-2} and 7.11 x 10^{-4} cm^{-2} respectively. The electrochemical effective area for the 18% SP/ABS and 18% SP ABC/PC were found to be 4.93 x 10^{-4} cm^{-2} and 4 x 10^{-4} cm^{-2} respectively. The electrochemical effective area of the SP blend with single polymer were found to be greater than that of the SP blend with two different polymers. This behaviour was may be because, with the addition of PC to ABS, the SP particles either came in between the grain boundaries or its concentration in one polymeric phase were increased.(56, 141, 142, 144) Consequently, the area for the charge transfer was decreased, which resulted in producing the low peak currents and active electrochemical area. Further, the change in the electrochemical behaviour of the CPC upon 3D printing was examined. The bulk filament (BF) of the polylactic acid (PLA) were prepared using the Nano-graphite (NG), Graphene nano-pellets, and the carbon black (SP) as a filler. The BF with different amount of the filler loading were produced. Under the cyclic voltammetric studies (following a process as explained earlier), the BF of all composites showed the higher peak currents as compared to the 3DEs, and the peak to peak separation for 3DE was greater as compared to their counter bulk filament (an example is shown in **Error! Reference source not found.**).

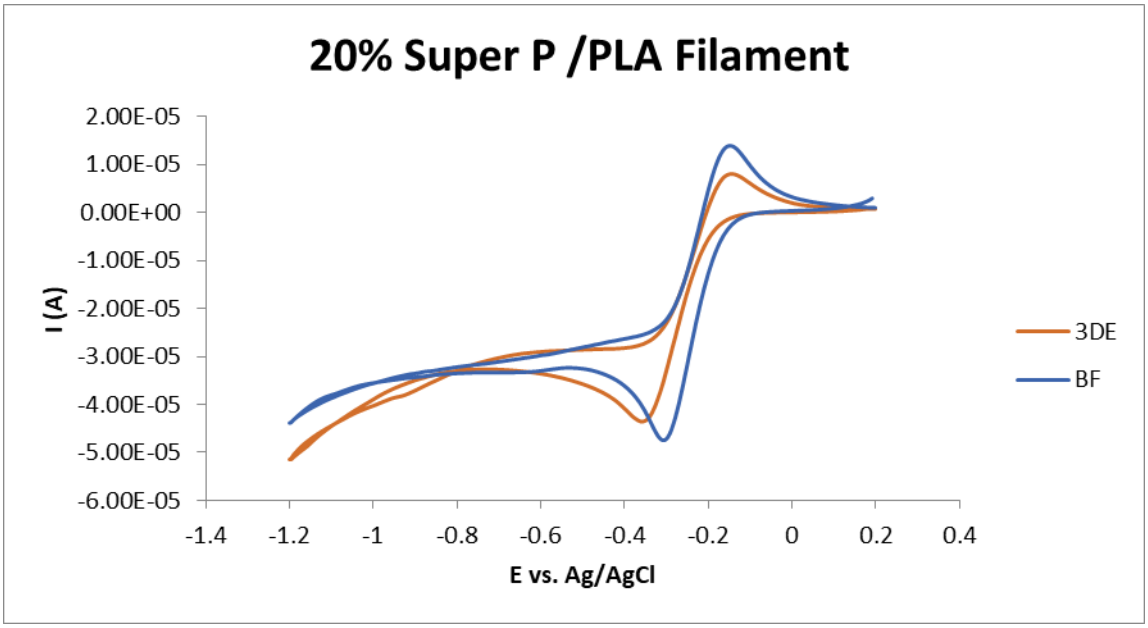

Figure 7.3 Comparison of the electrochemical response of 20% SP/PLA bulk filament (BF) and its 3D printed electrode (3DE) at 5 mVs^{-1}.

Foster(139) also published the same fact that the BF of the graphene based CPC showed a different electrochemical behaviour than its 3DE. This change in the behaviour was may be due to the redistribution of the filler particles when it was melted during the 3D printing. Here, the model proposed by Wesseling(145) for the percolation of CPC is useful to understand this phenomenon. The model explains that during mixing, the conductive filler particles get surrounded by the absorbing polymer layer (20nm). Below the percolation threshold, the filler particles are distributed evenly in the polymer phase. When the concentration reaches the percolation, the compression forces produced during mixing will destroy the adsorbed polymer layer of the particles, and they will start to percolate. (for detail see **Figure 2.2**). Similarly, when the filament was passed through the heated 3D printer's extruder, the agglomerated particles faced a redistribution. The primary clusters were started to break down into smaller groups which reduced the conductivity and peak currents. There was also a noticeable difference between the oxidation and reduction peak currents at the faster scan rate (as shown in **Figure 7.4**); which may be because of the CPC had a polarisation resistance. The individual particles encapsulated within the polymer, once charged to potential cannot be depolarised quickly.

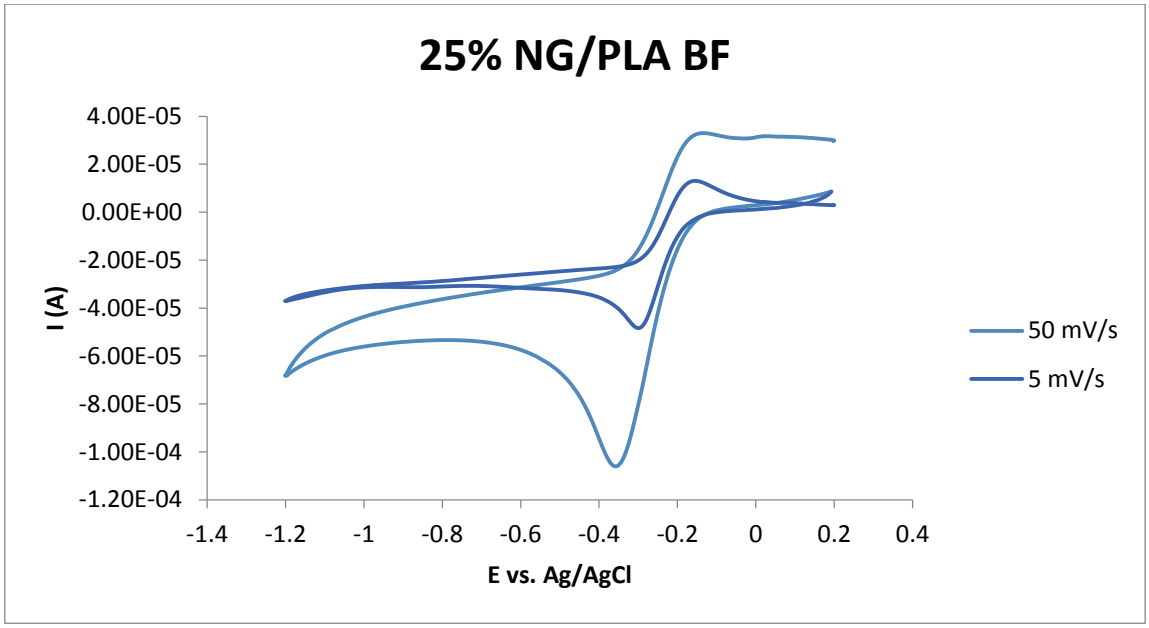

Figure 7.4 Cyclic voltammetric study of the 25% NG/PLA bulk filament at different scan rates.

The other possible reason for this type of response was that those particles which aiding the electron transfer by the quantum tunnelling effect were unable to change its potential quickly and were responsible for the polarisation resistance. Moreover, the graph between peak current vs scan rate for 20% SP-ABS (TF), 20% SP-PLA (BF), 20% NG- PLA (BF), and 20% SP-PLA (BF) showed the gradient close to 0.5 depicting the charge transfer occurred according to the semi-infinite linear diffusion model. The graph between peak current vs scan rate (I_p vs V) of different part of the same filament showed different values of the gradient and most of them are below 0.35 depicting the charge transfer is not solely governed by the diffusional process (data is available from **Table 7.5** - **Table 7.10**).(120, 140) The value of the gradient (I_p vs V) different parts of the filament designated as Tail1, Tail 2, and Mid of 20% Filler-(50%SP-50%Graphene)/ PLA showed values of 0.23, 0.04, and 0.33 respectively. These variable values may be due to the different distribution of the filler particles along the same filament which suggest the non-uniform characteristic along the length of the same CPC filament. All the produced bulk filaments showed a similar trend i.e., the values of the gradient (I_p vs V) from the different parts of the same filament were different and very few values were close to the 0.5. In FDM based printer, the filament is the initial source for 3D printing. Thus, exploring the uniformity of the BF was necessary. For this, the voltammetric experiments of the produced filament from three different parts were studied, i.e., from the mid and the tails. In this regard, we calculated the

heterogeneous rate transfer constant using the Nicholson method, and according to their proposed theory for the quasi-reversible system, the difference between peak potentials is proportional to the kinetic rate transfer constant.

$$\varphi = \sqrt{k^0 * [\frac{\pi DvF}{RT}]} \quad (7.4)$$

By rearranging this equation, we can get k^0. Where, *φ is a* kinetic parameter, and it is a function of the difference in peak potential. However, above equation holds its validity when the separation between peak potential lies between 57mVs^{-1} to 250mVs^{-1} and when peak seperation (ΔE_p) does not lie between this range then we can use equation 7.5 to find out the heterogenous electron transfer rate constant.(139)

$$k^0 = \lfloor 2.18(D\alpha nFv/RT)^{0.5} \rfloor exp^{[-(\frac{\alpha 2nF}{RT})*\Delta Ep]} \quad (7.5)$$

k^0 = electron transfer rate constant (cm/s)

D= diffusional constant (cm^2/s)

V= scan rate (V/s)

F= faraday constant (C/V)

T= temperature of the electrolyte (Kelvin)

R = ideal gas constant (J/mol. K)

α = constant whose value is 0.5

The hexammine-ruthenium (iii) chloride was used as a redox probe because its reduction is based on the one-electron transfer process and the electrode kinetics is unresponsive to the surface oxides.(146) The diffusion coefficient of the $Ru(NH_3)_6^{2+/-3}$ was used as 9.1 x 10^{-6} cm^2 s^{-1} throughout the calculations. The K^0 of the produced BF and their 3DEs are given in **Table 7.4** to **Table 7.10**. All different parts of the filament from mid and tails showed the variable values. For example, tail-1, middle, tail-2, and 3DE of the 20% SP/PLA showed the K^0 of 2.824 x 10^{-4}, 8.28 x 10^{-4}, 4.88 x 10^{-4} and 2.39 x 10^{-4} cm s^{-1} respectively. Interestingly, the 3DEs of the CPC with 15% filler loading showed no electrochemical response as

compared to their BF. These filaments were produced by using a mini extruder with the maximum capacity of 5 grams. The produced filaments were near to 24 inches in length, and their exact size was depended upon the volumetric ratio of the constituent of the CPC. However, the result suggested that the uniformity of the BF will be a challenge in future. In fact, this trend of non-uniformity was similar to the compression moulded samples, that under compression the particles get percolated easily.(147-150) When the polymer melt was in the mixing chamber, the pressure was high, and that polymer melt which was near to the extrusion die was under compression. Once the polymer started to flow from the nozzle, the pressure became low, and thus with the change in force, the agglomeration characteristics were changed throughout the filament. Recently, Patel(151) along with his co-worker found the directional influence of the printing on the electrochemical response. They compared the electrochemical behaviour of two structures with similar dimensions printed in a different direction using the FDM printer, i.e., vertically and horizontally built geometry. The vertically built structure of carbon black blended with acrylic butadiene styrene (ABS) showed better electrochemical activity as compared with the structure constructed in the horizontal direction.

Further, we compared the best-produced BF and 3DEs with the traditional. The traditional electrodes showed the faster heterogenous electron transfer rate constant as compared to the BF and 3DEs. The K^0 of the BF of 20% graphene/PLA and 20% SP/PLA composites were found to be 3.2×10^{-4} and 2.824×10^{-4} cm s^{-1} respectively. These values are comparable to that of the conventional electrodes as shown in **Table 7.3**. All these facts suggest that the 3D printers in the future can be employed in the production of the electrochemical architectures. However, this domain of additive manufacturing demands constant research and development; which are not limited to materials science but also required for the computation work in designing the complex algorithms.

Table 7.3 Comparison of the plastic based electrodes with some traditional electrodes regarding the heterogenous rate transfer constant. The cyclic voltametry experiments are

conducted using 1mM hexaammine-ruthenium (iii) chloride/0.1 M potassium chloride as a redox probe at selected scan rates within the range of 10-400 mVs^{-1}.

Electrode	Geometrical area (mm^2)	Counter/reference electrode	K^0 ($cm\ s^{-1}$)
Carbon-Screen printed electrode	7.7	Platinum/saturated calomel electrode	1.19×10^{-3}
Edge plane pyrolytic graphite	19.63	Platinum/saturated calomel electrode	7.0×10^{-3}
20% graphene- PLA bulk filament	69.12	Platinum/saturated calomel electrode	4.1×10^{-4}
20% graphene- PLA 3DE	7.7	Platinum/saturated calomel electrode	1.9×10^{-4}

Table 7.4 Results from the cyclic voltammetric experiments conducted on ABS and ABS-PC thin films using 1mM hexaammine-ruthenium (iii) chloride/0.1 M potassium chloride as a redox probe at selected scan rates within the range of 10-400 mVs^{-1}.

% filler (Super P-carbon black)	K^0	*Gradient* $\sqrt{v}$ *vs* I_P	*Gradient log (scan rate) vs* I_P
20	3.047×10^{-3}	9×10^{-4}	0.5086
18	1.402×10^{-3}	4×10^{-4}	0.3938
16	8.44×10^{-4}	3×10^{-4}	0.329
14	4.17×10^{-4}	2.888×10^{-4}	0.343
12	1.89×10^{-4}	2×10^{-4}	0.2385
ABS-PC			
20	7.64×10^{-4}	4×10^{-4}	0.3786
18	5.61×10^{-4}	3×10^{-4}	0.3545
16	5.61×10^{-4}	3×10^{-4}	0.3545
14	4.17×10^{-4}	2.7×10^{-4}	0.2753
12	1.45×10^{-4}	1.9×10^{-4}	0.3284

Table 7.5 Results from the cyclic voltammetric experiments conducted on 20% Super P/PLA and 20% Graphene/PLA CPC using 1mM hexaammine-ruthenium (iii) chloride/0.1 M potassium chloride as a redox probe at selected scan rates within the range of 10-400 mVs^{-1}.

Sample Designation	K^0	*v (scan rate) vs* I_P	*log (scan rate) vs log* I_P
20% Super P / PLA			
Filament Tail 1	2.824×10^{-4}	$y = -(2.3 \times 10^{-4})\ x - (1.9 \times 10^{-4})$	y = 0.3666x - 3.6656
Filament Tail 2	8.28×10^{-4}	$y = -(2.74 \times 10^{-4})\ x - (2.3 \times 10^{-4})$	y = 0.4146x - 3.5378
Filament Mid	4.88×10^{-4}	$y = -(2.25 \times 10^{-4})\ x - (2 \times 10^{-5})$	y = 0.3642x - 3.6667
3DE	2.39×10^{-4}	$y = -(1.58 \times 10^{-4})\ x - 1.406 \times 10^{-5}$	y = 0.3554x - 3.8314
20% Graphene / PLA			
Filament Tail 1	3.2×10^{-4}	$y = -(7.5 \times 10^{-4})\ x - (2 \times 10^{-5})$	y = 0.2379x - 4.1105
Filament Tail 2	4.8×10^{-4}	$y = -(1 \times 10^{-4})\ x - (2 \times 10^{-5})$	y = 0.269x - 4.001
Filament Mid	4.1×10^{-4}	$y = -(6.8 \times 10^{-4})\ x - (2 \times 10^{-5})$	y = 0.2175x - 4.1592
3DE	1.9×10^{-4}	$y = -(5.3 \times 10^{-4})\ x - (1.62 \times 10^{-5})$	y = 0.2273x - 4.2422

Table 7.6 Results from the cyclic voltammetric experiments conducted on 20% Filler-(50%NG-50%Graphene)/PLA and 20% Filler-(50%SP-50%Graphene)/PLA CPC using 1mM hexammine-ruthenium (iii) chloride/0.1 M potassium chloride as a redox probe at selected scan rates within the range of 10-400 mVs^{-1}.

Sample Designation	*K^0*	*$\sqrt{}$ (scan rate) vs I_P*	*log (scan rate) vs log I_P*
20% Filler-(50%NG-50%Graphene)/ PLA			
Filament Tail 1	4.5×10^{-4}	$y = -(3.8 \times 10^{-4})\ x - (1.720 \times 10^{-4})$	y = 0.1755x - 4.3489
Filament Tail 2	2.3×10^{-4}	$y = -(6.7 \times 10^{-4})\ x - (1.245 \times 10^{-4})$	y = 0.2962x - 4.1668
Filament Mid	1.8×10^{-4}	$y = -(6.661 \times 10^{-6})\ x - (1.337 \times 10^{-4})$	y = 0.2797x - 4.1764
3DE	4.7×10^{-4}	$y = -(9 \times 10^{-4})\ x - (1.5 \times 10^{-4})$	y = 0.2847x - 4.0717
20% Filler-(50%SP-50%Graphene)/ PLA			
Filament Tail 1	1.0×10^{-4}	$y = -(5.8 \times 10^{-4})\ x - (1.4 \times 10^{-5})$	y = 0.2306x - 4.2585
Filament Tail 2	4.2×10^{-4}	$y = -(9.2 \times 10^{-4})\ x - (1.6 \times 10^{-4})$	y = 0.0427x - 4.6833
Filament Mid	2.8×10^{-3}	$y = -(1.1 \times 10^{-4})\ x - (1.4 \times 10^{-4})$	y = 0.3399x - 3.9488
3DE	4.3×10^{-4}	$y = -(4.1 \times 10^{-4})\ x - (1.8 \times 10^{-4})$	y = 0.1694x - 4.3243

Table 7.7 Results from the cyclic voltammetric experiments conducted on 20% Filler-(50%NG-50%Graphene)/PLA and 20% Filler-(50%SP-50%Graphene)/PLA CPC using 1mM hexaammine-ruthenium (iii) chloride/0.1 M potassium chloride as a redox probe at selected scan rates within the range of 10-400 mVs^{-1}.

Sample Designation	*K^0*	*$\sqrt{}$ (scan rate) vs I_P*	*log (scan rate) vs log I_P*
20% Filler-(50%NG-50%Graphene)/ PLA			
Filament Tail 1	4.5×10^{-4}	$y = -(3.8 \times 10^{-4}) x - (1.7 \times 10^{-5})$	y = 0.1755x - 4.3489
Filament Tail 2	2.2×10^{-4}	$y = -(6.7 \times 10^{-4}) x - (1.2 \times 10^{-5})$	y = 0.2962x - 4.1668
Filament Mid	1.8×10^{-4}	$y = -(6.6 \times 10^{-5}) x - (1.3 \times 10^{-5})$	y = 0.2797x - 4.1764
3DE	4.7×10^{-4}	$y = -(9 \times 10^{-5}) x - (1.5 \times 10^{-5})$	y = 0.2847x - 4.0717
20% Filler-(50%SP-50%Graphene)/ PLA			
Filament Tail 1	1.0×10^{-3}	$y = -(5.9 \times 10^{-4}) x - (1.4 \times 10^{-4})$	y = 0.2306x - 4.2585
Filament Tail 2	4.2×10^{-4}	$y = -(9.2 \times 10^{-6}) x - (1.6 \times 10^{-4})$	y = 0.0427x - 4.6833
Filament Mid	2.8×10^{-3}	$y = -(1.8 \times 10^{-4}) x - (1.4 \times 10^{-4})$	y = 0.3399x - 3.9488
3DE	4.3×10^{-4}	$y = -(4.1 \times 10^{-5}) x - (1.9 \times 10^{-4})$	y = 0.1694x - 4.3243

Table 7.8 Results from the cyclic voltammetric experiments conducted on 20% Filler-(50%NG-50%Graphene)/PLA and 20% Filler-(50%SP-50%Graphene)/PLA CPC using 1mM hexaammine-ruthenium (iii) chlorid/0.1 M potassium chloride as a redox probe at selected scan rates within the range of 10-400 mVs^{-1}.

Sample Designation	*K^0*	*$\sqrt{}$ (scan rate) vs I_P*	*log (scan rate) vs log I_P*
20% Filler-(50%NG-50%Graphene)/ PLA			
Filament Tail 1	4.5×10^{-4}	$y = -(3.8 \times 10^{-5})\ x - (1.720 \times 10^{-5})$	y = 0.1755x - 4.3489
Filament Tail 2	2.27×10^{-4}	$y = -(6.7 \times 10^{-4})\ x - (1.2 \times 10^{-4})$	y = 0.2962x - 4.1668
Filament Mid	1.81×10^{-4}	$y = -(6.6 \times 10^{-3})\ x - (1.3 \times 10^{-4})$	y = 0.2797x - 4.1764
3DE	4.71×10^{-4}	$y = -(9.05 \times 10^{-4})\ x - (1.5 \times 10^{-4})$	y = 0.2847x - 4.0717
20% Filler-(50%SP-50%Graphene)/ PLA			
Filament Tail 1	1.0×10^{-3}	$y = -(5.9 \times 10^{-4})\ x - (1.4 \times 10^{-5})$	y = 0.2306x - 4.2585
Filament Tail 2	4.2×10^{-4}	$y = -(9.18 \times 10^{-4})\ x - (1.6 \times 10^{-5})$	y = 0.0427x - 4.6833
Filament Mid	2.8×10^{-3}	$y = -(1.8 \times 10^{-4})\ x - (1.4 \times 10^{-4})$	y = 0.3399x - 3.9488
3DE	4.3×10^{-4}	$y = -(4.1 \times 10^{-4})\ x - (1.8 \times 10^{-4})$	y = 0.1694x - 4.3243

Table 7.9 Results from the cyclic voltammetric experiments conducted on 20% NG/PLA and 25% NG / PLA CPC using 1mM hexaammine-ruthenium (iii) chloride/0.1 M potassium chloride as a redox probe at selected scan rates within the range of 10-400 mVs^{-1}.

Sample Designation	*K^0*	*$\sqrt{}$ (scan rate) vs I_P*	*log (scan rate) vs log I_P*
20% NG / PLA			
Filament Tail 1	1.3×10^{-4}	$y = -(2.9 \times 10^{-4}) x - (6.5 \times 10^{-5})$	y = 0.1767x - 4.6565
Filament Tail 2	3.1×10^{-4}	$y = -(5.8 \times 10^{-4}) x - (1.5 \times 10^{-5})$	y = 0.1767x - 4.6565
Filament Mid	4.2×10^{-4}	$y = -(1.2 \times 10^{-4}) x - (3.2 \times 10^{-5})$	y = 0.4228x - 3.9597
3DE	2.4×10^{-4}	$y = -(3 \times 10^{-4}) x - (1.9 \times 10^{-5})$	y = 0.1414x - 4.3956
25% NG / PLA			
Filament Tail 1	1.0×10^{-3}	$y = -(3 \times 10^{-4}) x - (1.9 \times 10^{-5})$	y = 0.4465x - 3.2789
Filament Tail 2	9.3×10^{-4}	$y = -(3.7 \times 10^{-4}) x - (2.7 \times 10^{-5})$	y = 0.4174x - 3.412
Filament Mid	3.1×10^{-3}	$y = -(2.5 \times 10^{-4}) x - (2.6 \times 10^{-5})$	y = 0.1414x - 4.395
3DE	3.1×10^{-3}	$y = -(1.4 \times 10^{-4}) x - (3.2 \times 10^{-5})$	y = 0.2954x - 3.7932

Table 7.10 Results from the cyclic voltammetry experiments conducted on 15% Filler (50% NG-50% Graphene) / PLA and 25% 15% SP/ PLA CPC using 1mM hexaammine-ruthenium (iii) chloride/0.1 M potassium chloride as a redox probe at selected scan rates within the range of 10-400 mVs^{-1}.

Sample Designation	*K^0*	*ν (scan rate) vs I_P*	*log (scan rate) vs log I_P*
15% Filler (50% NG-50% Graphene) / PLA			
Filament Tail 1	2.8×10^{-4}	$y = (9 \times 10^{-6})\, x - (1.8 \times 10^{-5})$	y = -0.0562x - 4.8773
Filament Tail 2	1.2×10^{-4}	$y = -(4.7 \times 10^{-6})\, x + (1 \times 10^{-5})$	y = -0.1318x - 5.2322
Filament Mid	3.2×10^{-4}	$y = -(6.3 \times 10^{-6})\, x - (1.8 \times 10^{-4})$	y = 0.2461x - 4.1656
3DE	*No appreciable conductance*		
15% SP/ PLA			
Filament Tail 1	3.4×10^{-4}	$y = -(8 \times 10^{-6})\, x - (2.3 \times 10^{-6})$	y = 0.417x - 4.1493
Filament Tail 2	1.3×10^{-4}	$y = -(1.9 \times 10^{-6})\, x + (1.5 \times 10^{-6})$	y = -0.0609x - 5.034
Filament Mid	9.4×10^{-5}	$y = (3 \times 10^{-5})\, x - (2 \times 10^{-4})$	y = -0.1019x - 5.0114
3DE	*No appreciable conductance*		

No.	Wavenumber (cm^{-1})	Functional group	Structure
1	3200-3000	Aromatic C—H	
2	2800-3000	Aliphatic C—H	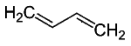
3	2190	Nitrile N≡C–	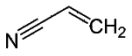
4	1770	Carbonyl C=O	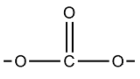
5	1620	Carbon double bond C=C	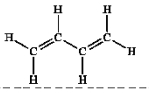
6	1490	Styrene ring stretching	
7	960	Butadiene C—H	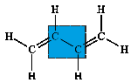
8	911	1,2 Butadiene C—H	

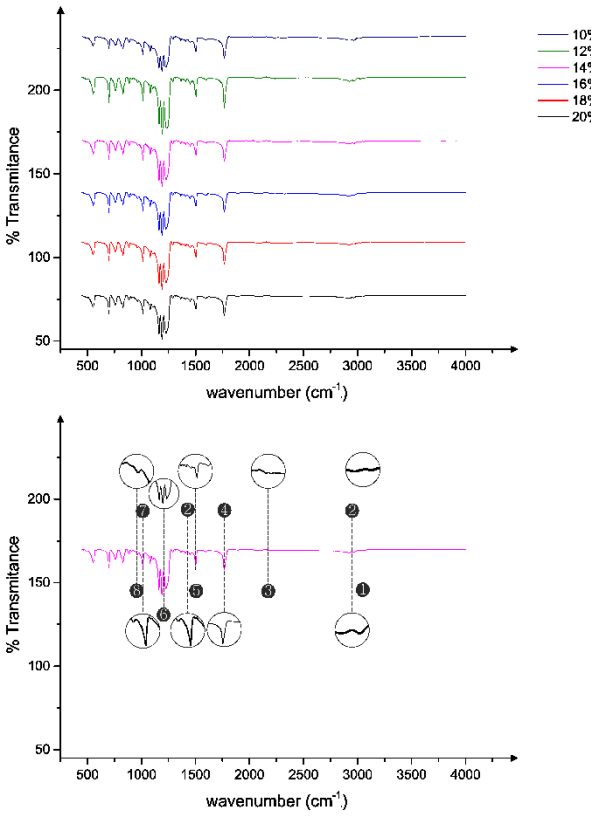

Figure 7.5 FTIR spectra of the composites based on ABS-PC polymeric blend with different percentages of the filler (SP-CB) within the range of 450-4000 cm^{-1}.

No.	Wavenumber (cm^{-1})	Functional group
1	3500	Hydroxyl —OH
2	2800-3000	Aliphatic C—H
3	1750	Carbonyl C=O
4	1450	Methyl —CH_3
5	1375	C—H deformation

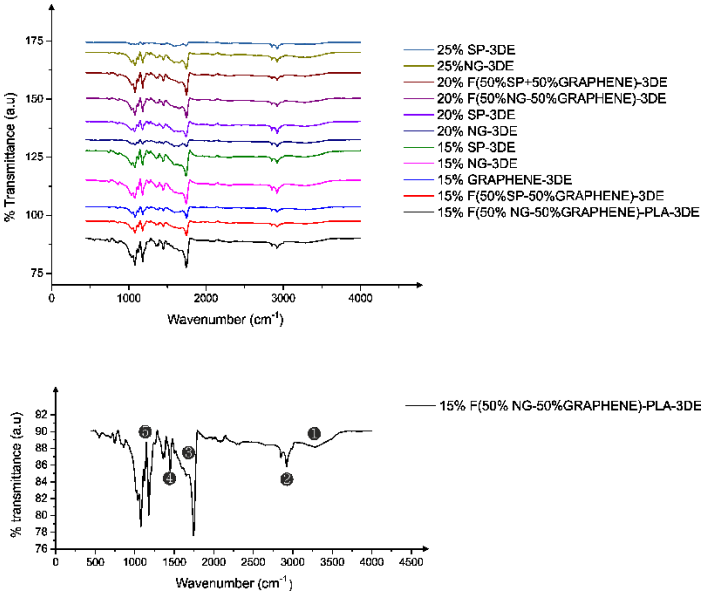

Figure 7.6 FTIR spectra of the composites based on PLA with different percentages of the filler (SP-CB) within the range of 450-4000 cm^{-1}.

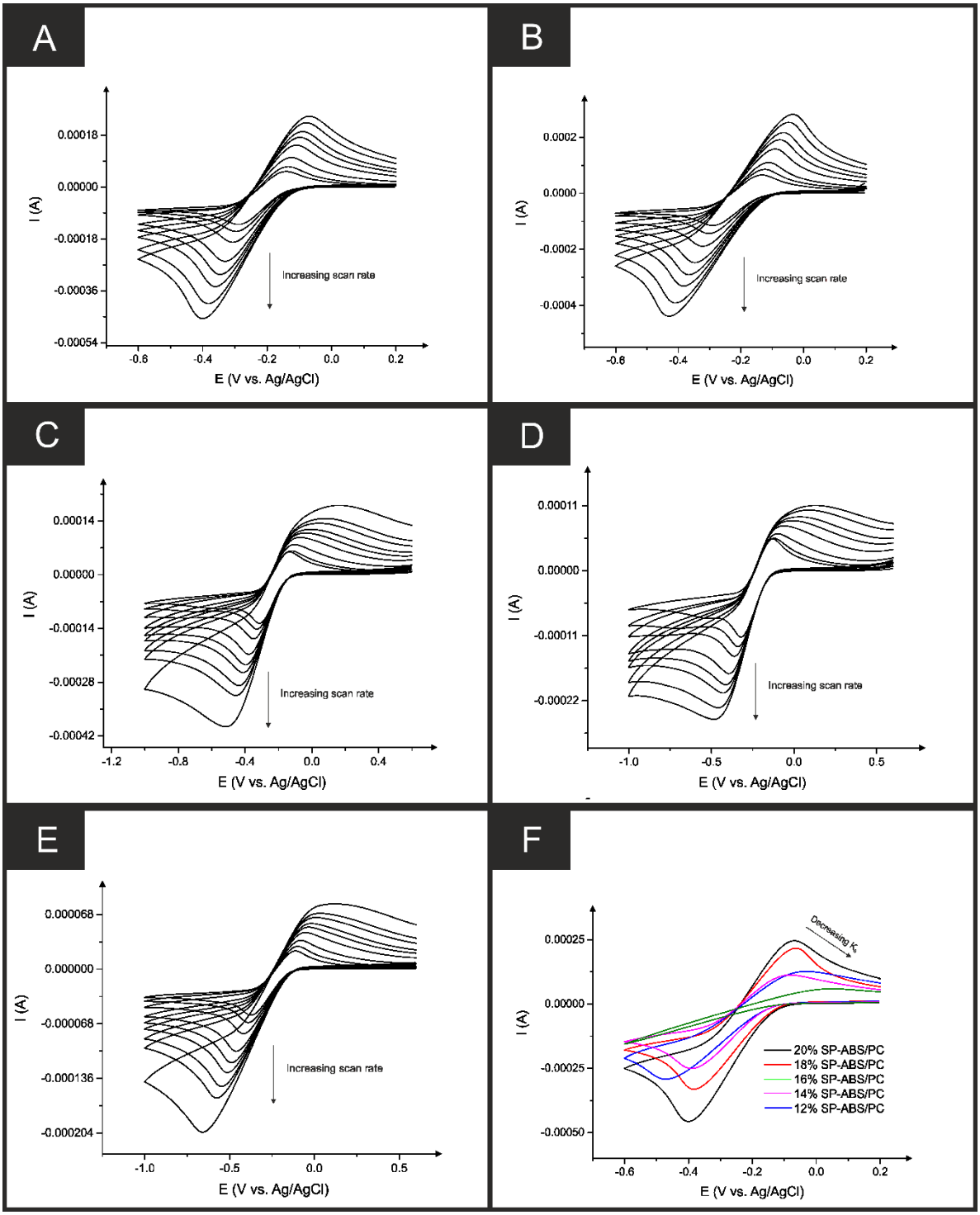

Figure 7.7 Cyclic voltammetric studies of (A) 20% Super P carbon black(SP)-ABS-PC, (B) 18% SP-ABS-PC, (C) 16% SP-ABS-PC, (D) 14% SP-ABS-PC, (E) 12% SP-ABS-PC and (F) comparison between all ABS-PC-CPC TF at 50 mVs^{-1}.

7.3 Conclusion:

Present work has contributed in exploring the electrochemistry of the 3D printed electrochemical architectures. The polylactic acid (PLA) blend with graphene, nano-graphite and super P carbon black were found to be a promising source for the manufacturing of the 3D printed electrochemical architectures. Moreover, the thin films with single polymer blend such as ABS filled with the electroactive material showed better electrochemical performance as compared with the CPC of ABS-PC. This trend validated that the individual polymer blend with the electroactive material is better for producing electrochemical architectures as compared to the blend with two immiscible polymers. The introduction of the immiscible polymer to a conductive polymeric composite (CPC) can enhance conductivity at the expense of the reduction in electrochemical area. The bulk CPC filament when passed through an extruder of the 3D printers, the filler particles face a redistribution which reduces the electrical conductivity. Therefore, the 3D printed ECA exhibits lower peak currents as compared with counter BF. Whereas, 3DEs showed low heterogenous rate transfer constant (towards hexammine-ruthenium (iii) chloride) and had a higher peak to peak separation in contrast with the counter traditional electrodes. When different parts of the BF were subjected to electrochemical studies, they showed different behaviours proving that the homogeneity of the 3DE will be a challenge in future.

7.4 Future Work:

The research contribution presented in this thesis demonstrated the electrochemical behaviour of 3D printed electrochemical architectures produced using FDM. The 3D printers can be employed as the production units capable of manufacturing the plastic-based electrodes for sensing and energy storage platforms. In the future, the produced electrodes will be evaluated as both for electroanalytical and energy storage applications.

8. References

1. Lipson H, Kurman M. Fabricated: The new world of 3D printing: John Wiley & Sons; 2013.
2. Gebhardt A, Hötter J-S. Additive Manufacturing. In: Gebhardt A, Hötter J-S, editors. Additive Manufacturing: Hanser; 2016. p. I-XX.
3. Marquardt T, Zheng E. History of 3D Printing.
4. Munaz A, Vadivelu RK, St. John J, Barton M, Kamble H, Nguyen N-T. Three-dimensional printing of biological matters. Journal of Science: Advanced Materials and Devices. 2016;1(1):1-17.
5. Lušić M, Barabanov A, Morina D, Feuerstein F, Hornfeck R. Towards zero waste in additive manufacturing: a case study investigating one pressurised rapid tooling mould to ensure resource efficiency. Procedia CIRP. 2015;37:54-8.
6. Canessa E, Fonda C, Zennaro M, Deadline N. Low--cost 3D printing for science, education and sustainable development. Low-Cost 3D Printing. 2013;11.
7. Ford S, Despeisse M. Additive manufacturing and sustainability: an exploratory study of the advantages and challenges. Journal of Cleaner Production. 2016;137:1573-87.
8. Kolomiets A, Popov Jr VV, Strokin E, Muller G, Kovalevsky A. Benefits of Additive Manufacturing for Industrial Design Development. Trends, Limitations and Applications. Global Journal of Research In Engineering. 2018.
9. Caffrey T, Wohlers T, Campbell R. Executive summary of the Wohlers Report 2016. © Wohlers Associates; 2016.
10. Zhang F, Wei M, Viswanathan VV, Swart B, Shao Y, Wu G, et al. 3D printing technologies for electrochemical energy storage. 2017;40:418-31.
11. Kruth J-P, Leu M-C, Nakagawa T. Progress in additive manufacturing and rapid prototyping. Cirp Annals. 1998;47(2):525-40.
12. Mueller B. Additive manufacturing technologies–Rapid prototyping to direct digital manufacturing. Assembly Automation. 2012;32(2).
13. Ngo TD, Kashani A, Imbalzano G, Nguyen KT, Hui D. Additive manufacturing (3D printing): A review of materials, methods, applications and challenges. Composites Part B: Engineering. 2018.
14. Bakhtiar SM, Butt HA, Zeb S, Quddusi DM, Gul S, Dilshad E. Chapter 10 - 3D Printing Technologies and Their Applications in Biomedical Science. In: Barh D, Azevedo V, editors. Omics Technologies and Bio-Engineering: Academic Press; 2018. p. 167-89.
15. Melocchi A, Parietti F, Loreti G, Maroni A, Gazzaniga A, Zema L. 3D printing by fused deposition modeling (FDM) of a swellable/erodible capsular device for oral pulsatile release of drugs. Journal of Drug Delivery Science and Technology. 2015;30:360-7.
16. Tian X, Jin J, Yuan S, Chua CK, Tor SB, Zhou KJAEM. Emerging 3D-printed electrochemical energy storage devices: a critical review. 2017;7(17):1700127.
17. Ambrosi A, Pumera M. 3D-printing technologies for electrochemical applications. Chemical Society Reviews. 2016;45(10):2740-55.
18. Lu D, Luo S, Wong C. Conductive polymer composites. Encyclopedia of Polymer Science and Technology. 2004.
19. Yang J, Liu Y, Liu S, Li L, Zhang C, Liu T. Conducting polymer composites: material synthesis and applications in electrochemical capacitive energy storage. Materials Chemistry Frontiers. 2017;1(2):251-68.
20. Carneiro OS, Silva AF, Gomes R. Fused deposition modeling with polypropylene. Materials & Design. 2015;83:768-76.
21. Bose R. A Geometric Morphometric Approach in Assessing Paleontological Problems in Atrypid Taxonomy, Phylogeny, Evolution and Ecology. Biodiversity and Evolutionary Ecology of Extinct Organisms: Springer; 2013. p. 1-9.
22. Ruqin Y, Sun L, Liang Y. Classification of materials. Data Handling in Science and Technology. 1995;15:155-79.

23. Van Krevelen DW, Te Nijenhuis K. Properties of polymers: their correlation with chemical structure; their numerical estimation and prediction from additive group contributions: Elsevier; 2009.
24. Rennie A. Thermoplastics and Thermosets. Mechanical Properties and Testing of Polymers: Springer; 1999. p. 248-.
25. Gnanasekaran K, Heijmans T, van Bennekom S, Woldhuis H, Wijnia S, de With G, et al. 3D printing of CNT- and graphene-based conductive polymer nanocomposites by fused deposition modeling. Applied Materials Today. 2017;9:21-8.
26. Langford WK. Achieving precise flow in fused deposition modeling extruders. Term Paper-Engineering Management. 2012;52.
27. Young RJ, Lovell PA. Introduction to polymers: CRC press; 2011.
28. Callister WD, Rethwisch DG. Materials science and engineering: John Wiley & Sons NY; 2011.
29. Rhee WM, Delustro FA, Berg RA. Crosslinked polymer compositions and methods for their use. Google Patents; 2000.
30. Graessley WW. Entangled linear, branched and network polymer systems—molecular theories. Synthesis and Degradation Rheology and Extrusion: Springer; 1982. p. 67-117.
31. Bates FS, Fredrickson GH. Block copolymer thermodynamics: theory and experiment. Annual review of physical chemistry. 1990;41(1):525-57.
32. Peters ST. Handbook of composites: Springer Science & Business Media; 2013.
33. Chawla KK. Composite Materials: Science and Engineering: Springer New York; 2013.
34. Barner-Kowollik C, Falkenhagen J, Gruendling T, Weidner S. Introduction: Wiley Online Library; 2008.
35. Smith WF, Hashemi J. Foundations of Materials Science and Engineering: McGraw-Hill; 2003.
36. Muc A, Barski M. Design of Particulate-Reinforced Composite Materials. Materials. 2018;11(2):234.
37. Lloyd D. Particle reinforced aluminium and magnesium matrix composites. International Materials Reviews. 1994;39(1):1-23.
38. Mallick PK. Fiber-Reinforced Composites: Materials, Manufacturing, and Design, Second Edition: Taylor & Francis; 1993.
39. Bishop SM, Curtis PT. Fibre reinforced composites. Google Patents; 1985.
40. Campbell FC. Structural Composite Materials: ASM International; 2010.
41. Cha KK. Composite Materials: Science and Engineering: Springer New York; 2013.
42. Lubin G, Peters ST. Handbook of Composites: Springer US; 1998.
43. Callister WD, Rethwisch DG. Materials Science and Engineering: An Introduction, 9th Edition: Ninth Edition: John Wiley and Sons, Incorporated; 2013.
44. Smith WF, Hashemi J. Foundations of materials science and engineering: McGraw-Hill; 2011.
45. Seymour RB. Polymer composites: VSP; 1990.
46. Zhang R, Agar JC, Wong C. Conductive polymer composites. Encyclopedia of Polymer Science and Technology. 2011.
47. Taherian R, Kausar A. Electrical Conductivity in Polymer-Based Composites: Experiments, Modelling and Applications: Elsevier - Health Sciences Division; 2018.
48. Radzuan NAM, Sulong AB, Sahari J. A review of electrical conductivity models for conductive polymer composite. International Journal of Hydrogen Energy. 2017;42(14):9262-73.
49. Kim YS. Electrical conductivity of segregated network polymer nanocomposites: Texas A & M University; 2010.
50. Grimmett G. What is Percolation? Percolation: Springer; 1999. p. 1-31.
51. Kirkpatrick S. Percolation and conduction. Reviews of modern physics. 1973;45(4):574.
52. Aharoni SM. Electrical resistivity of a composite of conducting particles in an insulating matrix. Journal of Applied Physics. 1972;43(5):2463-5.
53. Janzen J. On the critical conductive filler loading in antistatic composites. Journal of Applied Physics. 1975;46(2):966-9.

54. Huang JC. Carbon black filled conducting polymers and polymer blends. Advances in Polymer Technology: Journal of the Polymer Processing Institute. 2002;21(4):299-313.
55. Bueche F. Electrical resistivity of conducting particles in an insulating matrix. Journal of Applied Physics. 1972;43(11):4837-8.
56. Sumita M, Sakata K, Asai S, Miyasaka K, Nakagawa H. Dispersion of fillers and the electrical conductivity of polymer blends filled with carbon black. Polymer bulletin. 1991;25(2):265-71.
57. Wessling B, Volk H, Mathew W, Kulkarni V. Models for understanding processing properties of intrinsically conductive polymers. Molecular Crystals and Liquid Crystals. 1988;160(1):205-20.
58. Ihn T. Semiconductor Nanostructures: Quantum States and Electronic Transport: OUP Oxford; 2010.
59. Jing X, Zhao W, Lan L. The effect of particle size on electric conducting percolation threshold in polymer/conducting particle composites. Journal of materials science letters. 2000;19(5):377-9.
60. Bloor D, Donnelly K, Hands P, Laughlin P, Lussey D. A metal–polymer composite with unusual properties. Journal of Physics D: Applied Physics. 2005;38(16):2851.
61. Setton R, Bernier P, Lefrant S. Carbon Molecules and Materials: Taylor & Francis; 2002.
62. Sharon M. Carbon nanoforms and applications: McGraw-Hill; 2010.
63. Donnet JB. Carbon Black: Science and Technology, Second Edition: Taylor & Francis; 1993.
64. Donnet J-B. Carbon black: science and technology: CRC Press; 1993.
65. Biscoe J, Warren B. An X-Ray Study of Carbon Black. Journal of Applied Physics. 1942;13(6):364-71.
66. Donnet J-BX. Carbon black: science and technology: CRC Press; 1993.
67. Zhang W, Dehghani-Sanij AA, Blackburn RS. Carbon based conductive polymer composites. Journal of materials science. 2007;42(10):3408-18 %@ 0022-2461.
68. Sichel EK. Carbon black-polymer composites: the physics of electrically conducting composites: M. Dekker; 1982.
69. Huang JC. Carbon black filled conducting polymers and polymer blends. Advances in Polymer Technology. 2002;21(4):299-313 %@ 1098-2329.
70. Gul VE. Structure and Properties of Conducting Polymer Composites: Taylor & Francis; 1996.
71. Miyasaka K, Watanabe K, Jojima E, Aida H, Sumita M, Ishikawa K. Electrical conductivity of carbon-polymer composites as a function of carbon content. Journal of Materials Science. 1982;17(6 %@ 1573-4803):1610-6.
72. Sumita M, Abe H, Kayaki H, Miyasaka K. Effect of melt viscosity and surface tension of polymers on the percolation threshold of conductive-particle-filled polymeric composites. Journal of Macromolecular Science—Physics. 1986;25(1-2):171-84 %@ 0022-2348.
73. Tchoudakov R, Breuer O, Narkis M, Siegmann A. Conductive polymer blends with low carbon black loading: polypropylene/polyamide. Polymer Engineering & Science. 1996;36(10):1336-46 %@ 548-2634.
74. Grunlan JC. Carbon Black-filled Polymer Composites: Property Optimization with Segregated Microstructures: University of Minnesota; 2001.
75. Díez EÁ. Effect of Extrusion on the Electrical, Mechanical and Rheological Properties of an Ethylene Butylacrylate/Carbon Black/Graphite Nanoplatelets Nanocomposite. 2014.
76. Silviya E, Varma S, Unnikrishnan G, Thomas S. 4-Compounding and mixing of polymers. Advances in Polymer Processing: Woodhead Publishing. 2009:71-105.
77. Consortium P. Introduction to Conductive Polymer Composites: Smithers Information Limited; 2011.
78. Bigg DM. An investigation of the effect of carbon black structure, polymer morphology, and processing history on the electrical conductivity of carbon-black-filled thermoplastics. Journal of Rheology. 1984;28(5):501-16 %@ 0148-6055.
79. Brydson JA. Plastics materials: Butterworth-Heinemann; 1999.
80. Olabisi O, Adewale K. Handbook of Thermoplastics: Taylor & Francis; 1997.

81. Bernhardt EC. Processing of Thermoplastic Materials: Robert E. Krieger Publishing Company; 1974.
82. Rupprecht L. Conductive Polymers and Plastics: In Industrial Applications: Elsevier Science; 1999.
83. Qattawi A, Alrawi B, Guzman A. Experimental optimization of fused deposition modelling processing parameters: a design-for-manufacturing approach. Procedia Manufacturing. 2017;10:791-803.
84. Rothon R, Limited RT. Particulate-filled Polymer Composites: Rapra Technology; 2003.
85. DeArmitt C, Hancock M. Particulate-Filled Polymer Composites2003. 357-424 p.
86. Brydson JA. Flow properties of polymer melts: Van Nostrand Reinhold Co.; 1970.
87. Shenoy AV. Rheology of filled polymer systems: Springer Science & Business Media; 2013.
88. Mallick PK. Processing of Polymer Matrix Composites: Processing and Applications: CRC Press; 2017.
89. Boyard N. Heat Transfer in Polymer Composite Materials: Forming Processes: Wiley; 2016.
90. Bernhardt E. Processing of Thermoplastic Materials. Bernhardt: Reinhold; 1959.
91. DeArmitt C, Rothon R. Fillers and surface treatment. Plastics, Additives and Compounding. 2002;4(5):12-4 %@ 1464-391X.
92. Wypych G. Handbook of fillers: Elsevier; 2016.
93. Huang X, Zhi C. Polymer Nanocomposites: Electrical and Thermal Properties: Springer International Publishing; 2016.
94. Mark JE. Physical Properties of Polymers Handbook: Springer New York; 2007.
95. Astrom BT. Manufacturing of Polymer Composites, 1997. London: Chapman & Hall.
96. Gnanasekaran K, Heijmans T, van Bennekom S, Woldhuis H, Wijnia S, Friedrich H. 3D printing of CNT-and graphene-based conductive polymer nanocomposites by fused deposition modeling. Applied Materials Today. 2017;9:21-8.
97. Subramanian MN. Introduction to Polymer Compounding: Raw Materials: Smithers Rapra Technology; 2014.
98. Mark HF. Encyclopedia of polymer science and technology, concise: John Wiley & Sons; 2013.
99. Berlin AA, Rogovina SZ, Zaikov GE. Additives in Polymers: Analysis and Applications: Apple Academic Press; 2016.
100. Rothon RN. Particulate-filled polymer composites: Longman Scientific & Technical; 1995.
101. Shooter KV, Tabor D. The frictional properties of plastics. Proceedings of the Physical Society Section B. 1952;65(9):661 %@ 0370-1301.
102. Denn MM. Polymer melt processing: foundations in fluid mechanics and heat transfer: Cambridge University Press; 2008.
103. Tadmor Z, Gogos CG. Principles of polymer processing: John Wiley & Sons; 2013.
104. Rwei SP, Horwatt SW, Manas-Zloczower I, Feke DL. Observation and Analysis of Carbon Black Agglomerate Dispersion in Simple Shear Flows. International Polymer Processing. 1991;6(2):98-102 %@ 0930-777X.
105. Tadmor Z. Forces in dispersive mixing. Industrial & Engineering Chemistry Fundamentals. 1976;15(4):346-8 %@ 0196-4313.
106. Latinen GA. Devolatilization of viscous polymer systems. ACS Publications; 1962.
107. Pearson JRX. Mechanics of polymer processing: Springer Science & Business Media; 1985.
108. Crow DR. Principles and Applications of Electrochemistry: Springer US; 1994.
109. Zoski CG. Handbook of Electrochemistry: Elsevier Science; 2007.
110. Bockris JOM, Conway BE, White RE. Modern aspects of electrochemistry: Springer Science & Business Media; 2012.
111. Callister Jr WD, Rethwisch DG. Fundamentals of materials science and engineering: an integrated approach: John Wiley & Sons; 2012.
112. Plieth W. Electrochemistry for Materials Science: Elsevier Science; 2008.

113. Donbrow M. Instrumental Methods in Analytical Chemistry: Electrochemical methods: Pitman; 1966.
114. Ives DJG. Reference Electrodes: Theory and Practice: Acad. Press; 1969.
115. Wang JX. Analytical electrochemistry: John Wiley & Sons; 2006.
116. Surhone LM, Timpledon MT, Marseken SF. Nernst Equation: VDM Publishing; 2010.
117. Scholz F. Electroanalytical methods: Springer; 2010.
118. Brownson DAC, Banks CE. Interpreting electrochemistry. The Handbook of Graphene Electrochemistry: Springer; 2014. p. 23-77.
119. Holze R. Experimental Electrochemistry: Wiley; 2009.
120. Compton RG, Banks CE. Understanding Voltammetry: Imperial College Press; 2011.
121. Scholz F, Bond AM, Compton RG, Fiedler DA, Inzelt G, Kahlert H, et al. Electroanalytical methods: guide to experiments and applications : with 100 figures and 31 tables: Springer; 2002.
122. Gosser DK. Cyclic Voltammetry: Simulation and Analysis of Reaction Mechanisms: Wiley; 1993.
123. Brumleve TR, Buck RP. Numerical solution of the Nernst-Planck and Poisson equation system with applications to membrane electrochemistry and solid state physics. Journal of Electroanalytical Chemistry and Interfacial Electrochemistry. 1978;90(1):1-31 %@ 0022-728.
124. Zmorp. https://zmorph3d.com.
125. Scientific TF. https://thermofisher.com/.
126. Brownson DA, Munro LJ, Kampouris DK, Banks CE. Electrochemistry of graphene: not such a beneficial electrode material? Rsc Advances. 2011;1(6):978-88.
127. Li J, Chen F, Yang L, Jiang L, Dan Y. FTIR analysis on aging characteristics of ABS/PC blend under UV-irradiation in air. Spectrochimica Acta Part A: Molecular and Biomolecular Spectroscopy. 2017;184:361-7 %@ 1386-425.
128. Lasprilla AJR, Martinez GAR, Hoss B. Synthesis and characterization of poly (lactic acid) for use in biomedical field. Chem Eng. 2011;24:985-90.
129. Mehta R, Kumar V, Bhunia H, Upadhyay SN. Synthesis of poly (lactic acid): a review. Journal of Macromolecular Science, Part C: Polymer Reviews. 2005;45(4):325-49 %@ 1532-797.
130. Mofokeng JP, Luyt A, Tábi T, Kovács J. Comparison of injection moulded, natural fibre-reinforced composites with PP and PLA as matrices. Journal of Thermoplastic Composite Materials. 2012;25(8):927-48.
131. Yu J, Wang N, Ma X. Fabrication and characterization of poly (lactic acid)/acetyl tributyl citrate/carbon black as conductive polymer composites. Biomacromolecules. 2008;9(3):1050-7.
132. Cardenas G, Miranda SP. FTIR and TGA studies of chitosan composite films. Journal of the Chilean Chemical Society. 2004;49(4):291-5.
133. Foo CY, Lim HN, Mahdi MA, Wahid MH, Huang NM. Three-Dimensional Printed Electrode and Its Novel Applications in Electronic Devices. Scientific reports. 2018;8(1):7399.
134. You X, Yang J, Feng Q, Huang K, Zhou H, Hu J, et al. Three-Dimensional Graphene-Based Materials by Direct Ink Writing Method for Lightweight Application. 2018.
135. Cheng TS, Nasir MZM, Ambrosi A, Pumera MJAMT. 3D-printed metal electrodes for electrochemical detection of phenols. 2017;9:212-9.
136. Foster CW, Down MP, Zhang Y, Ji X, Rowley-Neale SJ, Smith GC, et al. 3D printed graphene based energy storage devices. 2017;7:42233.
137. Manzanares Palenzuela CL, Novotný F, Krupička P, Sofer Zk, Pumera MJAc. 3D-Printed Graphene/Polylactic Acid Electrodes Promise High Sensitivity in Electroanalysis. 2018;90(9):5753-7.
138. Banks CE, Foster CW, Kadara RO. Screen-Printing Electrochemical Architectures: Springer International Publishing; 2015.
139. Foster CW, Down MP, Zhang Y, Ji X, Rowley-Neale SJ, Smith GC, et al. 3D Printed Graphene Based Energy Storage Devices. Scientific Reports. 2017;7:42233 %@ 2045-2322.
140. Wang J. Analytical Electrochemistry: Wiley; 2006.
141. Tchoudakov R, Breuer O, Narkis M, Siegmann A. Conductive polymer blends with low carbon black loading: polypropylene/polyamide. Polymer Engineering & Science. 1996;36(10):1336-46.

142. Breuer O, Tchoudakov R, Narkis M, Siegmann A. Segregated structures in carbon black-containing immiscible polymer blends: HIPS/LLDPE systems. Journal of applied polymer science. 1997;64(6):1097-106.
143. Gubbels F, Blacher S, Vanlathem E, Jérôme R, Deltour R, Brouers F, et al. Design of electrical composites: determining the role of the morphology on the electrical properties of carbon black filled polymer blends. Macromolecules. 1995;28(5):1559-66.
144. Gubbels F, Jérôme R, Teyssie P, Vanlathem E, Deltour R, Calderone A, et al. Selective localization of carbon black in immiscible polymer blends: a useful tool to design electrical conductive composites. Macromolecules. 1994;27(7):1972-4.
145. Wessling B, Volk H, Mathew WR, Kulkarni VG. Models for understanding processing properties of intrinsically conductive polymers. Molecular Crystals and Liquid Crystals. 1988;160(1):205-20 %@ 1044-859.
146. Randviir EP, Brownson DA, Gómez-Mingot M, Kampouris DK, Iniesta J, Banks CEJN. Electrochemistry of Q-graphene. 2012;4(20):6470-80.
147. Kalaitzidou K, Fukushima H, Drzal LT. A route for polymer nanocomposites with engineered electrical conductivity and percolation threshold. Materials. 2010;3(2):1089-103.
148. Park SB, Lee MS, Park M. Study on lowering the percolation threshold of carbon nanotube-filled conductive polypropylene composites. Carbon Lett. 2014;15(2):117-24.
149. Király A, Ronkay F. Effect of processing technology on the morphological, mechanical and electrical properties of conductive polymer composites. Journal of Polymer Engineering2013. p. 691.
150. Hao X, Gai G, Yang Y, Zhang Y, Nan C-w. Development of the conductive polymer matrix composite with low concentration of the conductive filler. Materials Chemistry and Physics. 2008;109(1):15-9.
151. Hamzah HHB, Keattch O, Covill D, Patel BAJSr. The effects of printing orientation on the electrochemical behaviour of 3D printed acrylonitrile butadiene styrene (ABS)/carbon black electrodes. 2018;8(1):9135.